ANALYSIS OF ELECTROKINETIC FLOW IN MICROFLUIDIC CHIPS

By

Sanket Aryal

Submitted in Partial Fulfillment of the Requirements

for the degree of

Master of Science in Engineering

in the

Mechanical Engineering Program

Youngstown State University

May 2012

ANALYSIS OF ELECTROKINETIC FLOW IN MICROFLUIDIC CHIPS

Sanket Aryal

I hereby release this thesis to the public. I understand that this thesis will be made available from the Ohio LINK ETD Center and the Maag Library Circulation Desk for public access. I also authorize the University or other individuals to make copies of this thesis as needed for scholarly research.

Signature:

Sanket Aryal, Student Date

Approvals:

Dr. Yogendra M. Panta, Thesis Advisor Date

Dr. Hans Tritico, Committee Member Date

Dr. Pedro Cortes, Committee Member Date

Dr. Peter J. Kasvinsky, Dean of School of Graduate Studies and Research Date

ABSTRACT

Miniaturization and integration of conventional bioassay laboratory procedures into the micro-fabricated Lab-On-Chips (LOCs), usually referred to as ”Micro Total Analysis (μTAS) systems”, have tremendous impacts in the fields of genomics, proteomics, and other clinical analysis. Electrokinetically driven flow offers efficiently and effectively to control flow in micro devices without a need for any mechanical components. These bioanalytical microsystems utilize electrokinetic mobility including electroosmosis and electrophoresis modes for transport, mixing, manipulation, separation and detection of sample analytes. LOCs are already proven to significantly reduce analysis time and sample volume sizes without requiring a skilled worker to operate. In addition, LOCs are inexpensive, versatile, robust as well as portable**.**

At the solid surfaces of the microchannel walls, an oppositely charged thin layer is formed separate from the bulk solutions of the sample analytes and buffer solutions. This thin layer is referred to as an “Electrical Double Layer (EDL)” or simply called “Debye’s Thickness Layer”. Based on the type and material of the electrode surface, it is formed either by negatively or positively charged ionic groups from the bulk solution at the wall’s surfaces. Using commercially available finite element software, called “COMSOL Multiphysics”, the electric field is modeled in such a way that it displaces EDL formed by ionic liquid leading to generate an electrokinetic flow in the microchannel. *MEMS (Micro-electromechanical systems) and Chemical Engineering Modules* of COMSOL are employed to model, physics set up, and simulate the ionic fluid flow for the analysis of fluid propulsion and chemical mass transport for the various physical models of microchips. The ionic fluid concentrations and velocities are plotted against the potential

differences across the sample inlet vs. the outlet and across the buffer inlet vs. the outlet, respectively. Based on the COMSOL Multiphysics simulation results, it was concluded that the T-shaped microfluidic chip with a narrowed cross sectional area at the analysis chamber has maximum ionic velocity that increases with increase in electric potential for the EDL (Zeta potential) formed. Ionic concentration could be accumulated at the outlet by achieving higher concentrations with the electrophoresis mode. Thus, velocity and concentration distributions in the microfluidic chip could be manipulated by varying shape and size of the chips, varying potential differences between two inlets vs. outlet and varying zeta potential at the microchannel wall. In this thesis work, LOCs with microchannels were analyzed with varying parameters of electrical, chemical, and physical properties and proven their effects on the concentrations and the velocities of the sample analytes.

ACKNOWLEDGEMENTS

I would like to express my deepest gratitude to my advisor Dr. Yogen M. Panta for the continuous support of my study and research as a graduate student. His guidance, extreme patience and long suffering, ideas, and opinions helped me immensely throughout this thesis work. In addition, my special thanks go to Dr. Hans Tritico and Dr. Pedro Cortes for having accepted the task of serving on my thesis committee and helping me in proofreading and providing important suggestions. I would also like to acknowledge Dr. Chester R. Cooper for his continuous support for my graduate studies through the "YSU-Center for Applied Chemical Biology (CACB)". My classmates and dear friends Param Adhikari, Jay Devkota, Lin Wei, Munindra Khadka, Salim Baksh and Darshan Baral are thankful for their unforgettable friendly support and help.

I would also like to give my endless thanks to my parents, my sisters and my wife for their encouragement and support. Without their love and support, none of this work would have ever been possible.

Lastly I want to convey my appreciation to the YSU-Department of Mechanical and Industrial Engineering for providing me resources to accomplish this research.

This thesis work was partially supported by YSU-Center for Applied Chemical Biology (CACB).

TABLE OF CONTENTS

LIST OF FIGURES

LIST OF TABLES

CHAPTER 1

INTRODUCTION

1.1 Lab on chip and its applications

Recent years have witnessed significant advances in the microfluidics field and have seen decent development on Lab-on-chip (LOC) technologies for a number of biochemical analysis. Lab-on-chip devices promise many novel applications concerning the transport of the liquid samples and other solutions in the order of micro-scale dimensions. A lab-on-chip is a device that integrates one or several laboratory functions on a single chip of only millimeters to a few square centimeters in size. They also save the sample size required to be analyzed from nano-liters to several microliters. Lab-on-chip devices are a subset of MEMS devices and often indicated by "Micro Total Analysis Systems" (μTAS) as well. Microfluidics is a broader term that also describes mechanical flow control devices like micro-pumps and micro-valves or micro-sensors like flowmeters and viscometers. Some of merits of microfluidic chips or microscale total analysis systems (μ TAS) are reducing consumption of samples and reagents, shortening analysis times, having greater sensitivity, portability and disposability compared to traditional laboratory apparatus. In this thesis, COMSOL Multiphysics software was used to investigate and understand the effectiveness of transport modes of ionic sample analytes for a variety of microfluidic chips based on inlets and one outlet.

1.2 Modes of flow motion in microfluidic chips

The purpose of this section is to illustrate several modes of fluid motion in micro/nano-fluidic chips. A summary of various means of fluid propulsion along with their brief description, advantages and disadvantages as shown in Table 1.1

Table 1.1 Summary of various means of fluid propulsion

Means	Description	Advantages	Disadvantages
Pressure	Fluid motion is induced by pressure difference.	High flow rate; No moving part	Need a mechanical pump; High pressure
Surface tension	Fluid motion is induced by surface tension.	No external driving force; No moving part	Difficult to control the flow rate and direction
Centrifugal force	The device is placed on a rotating platform.	High flow rate	Fluids move only in one direction
Buoyancy	Fluid motion is induced by the dependence of fluid density on the temperature variations.	Self-accurate; No moving part;	Large temperature variations are required.
Magneto-hydrodynamics (MHD) (*Panta et al, 2008, 2009, 2010*)	The motion is induced by the interactions between electric and magnetic fields.	Low cost; Low electric field; Reasonable flow rates; No moving part.	Electrode erosion; Bubble formation; Only certain fluids will work.
Electrokinetic	***Fluid motion is induced by electrostatic force.***	***Uniform velocity*** ***No moving part***	***Low flow rate;*** ***High electric field;*** ***Depends on the characteristics of the liquid-solid interface***

1.3 Fundamentals of electrokinetic flow

Electrokinetic flow covers in principle the transport of liquids (electroosmosis) and analytes samples (electrophoresis) in response to an electric field. Both motions are associated with the electric double layer that is formed spontaneously at the solid–liquid interface in which there is a net charge density. Electrophoresis is the simple drift of ions caused by an applied electric field. Electroosmosis describes the motion of electrolyte liquids with respect to a fixed wall that results when an electric field is applied parallel to the surface.

1.3.1 Electroosmosis

If the walls of a microchannel have an electric charge, as most surfaces do, an electric double layer of counter ions will form at the walls. When an electric field is applied across the channel, the ions in the double layer move towards the electrode of opposite polarity. This creates motion of the fluid near the walls and transfers via viscous forces into convective motion of the bulk fluid. If the channel is open at the electrodes, as is most often the case, the velocity profile is uniform across the entire width of the channel.

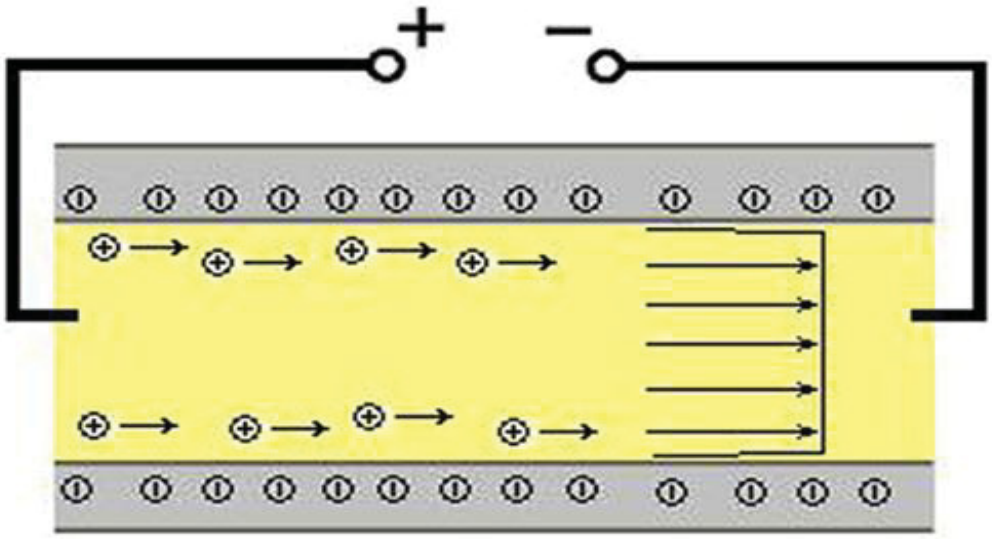

Figure 1.1 Flow velocity profile calculated for electroosmotic pumping in an open channel (*http://www.bioscience.org/2009/v14/af/3500/figures.htm*)

The most common simplification encountered in electroosmotic flow analysis is the "Helmholtz-Smoluchowski" approximation. To derive this we begin by eliminating the non-linear and transient terms of Navier-Stokes equation as shown in equation 1.1 and assume that the pressure gradient ∇p is zero everywhere.

$$\rho\left[\frac{\partial u}{\partial t}+(u.\nabla)u\right]=-\nabla p+\mu\nabla^2 u+\rho_e E \qquad \text{.....(1.1)}$$

where, μ denotes the dynamic viscosity (Pa·s), u is the velocity (mm/s), E is the electric field intensity (V), ρ denotes the fluid's density (kg/m^3), p is the pressure (Pa).

The latter of these assumptions is generally valid for pure electroosmotic flow (no applied pressure) with uniform surface (ς-potential) and solution (viscosity and conductivity) properties. These assumptions yield,

$$\eta \frac{d^2 v_x}{dy^2} - \varepsilon_w \varepsilon_o \frac{d^2 \psi}{dy^2} E = 0 \qquad \text{.....(1.2)}$$

This equation was further integrated with respect to *y* twice and apply the condition that as y $\rightarrow \infty$, $dv_x / dy = 0$, and $d\psi / dy = 0$, and that at y = 0 (i.e. the shear plane), $\psi = \zeta$. Following this procedure and considering the region outside the double layer $\psi = 0$ yields,

$$v_x = v_{eo} = \frac{\varepsilon_w \varepsilon_o \varsigma}{\eta} E_X \qquad \text{.....(1.3)}$$

which is commonly referred to as the Helmholtz-Smoluchowski equation and is descriptive of a plug flow velocity profile. Commonly, the terms which proceed E_X in equation 1.3 are expressed as a single linear proportionality coefficient between v_{eo} and E_X referred to as the electroosmotic mobility, $\mu_{eo} = -\frac{\varepsilon_w \varepsilon_o \varsigma}{\eta}$.

1.3.2 Electrophoresis

Electrophoresis involves separation of molecular analytes on the basis of their migration speed response to an applied electric field shown in equation 1.4. Considering drag on the moving analytes due to viscosity of the aqueous solution with low Reynolds number and moderate electric field strength E, the velocity of the analytes v is simply proportional to

the applied electric field. Thus induced mobility for the analytes, called as electrophoretic mobility, μ_{eo} defined as

$$\mu_{eo} = \frac{v}{E} \qquad \text{……..……(1.4)}$$

According to Helmholtz-Smoluchowski's (1903) theory of electrophoresis $\mu_{eo} = -\frac{\varepsilon_r \varepsilon_o \varsigma}{\eta}$

and $v_{eo} = -\frac{\varepsilon_w \varepsilon_o \varsigma}{\eta} E$ .....(1.5)

where, ε_r: dielectric constant of medium (water), ε_o: Permittivity of free space, η: dynamic viscosity of water.

This is only valid for thin double layer and does not include the Debye length K^{-1}. However, Debye length is only a few nanometers for a aqueous solutions medium and the Smoluchouski's theory is still valid. The theory neglects surface conducting on the walls expressed by Dunkin number. Du<<1.

1.4 Electric Double Layer (EDL)

An *Electrical Double Layer (EDL)* is a very thin region of non-zero net charge density near a two phase interface (for the cases of interest here, typically a solid-liquid interface). It is generally the result of adsorption or desorption of charged species from the surface and the resulting rearrangement of the local free ions in solution so as to maintain overall electro-neutrality. As shown in Figure 1.2, the diffuse region of the EDL decays roughly exponentially into the bulk solution with a depth characterized by the inverse of the Debye-Huckel parameter (1/κ). The penetration depth of the diffuse EDL

can vary from a few tenths of nanometers to over a micrometer, depending on the ionic strength of the bulk phase solution.

When an electric field is applied perpendicular to the decay of the EDL (or equivalently parallel with the surface), the surplus of either positive or negative ions results in a net body force on the fluid proportional to the local net charge density. The resulting velocity profile consists of a region of very high shear rate near the surface where the velocity increases from zero at the shear plane to its bulk phase velocity, v_{eo} at the edge of the EDL. The proportionality between v_{eo} and the strength of the electric field, E_x, is given by the electroosmotic mobility, μ_{eo}, which is a function of both surface and solution phase properties. Unlike pressure driven flow, uniform electroosmotic flow exhibits a flat or "plug flow" velocity profile outside the double layer region.

The popularity of electroosmotic flow as a primary transport mechanism in microfluidic devices is largely the result of the simplicity of its implementation and the uniqueness of this velocity profile. In the classic example, the near flat velocity profile serves to minimize sample dispersion in capillary electrophoresis systems, thereby facilitating highly efficient analytical separations (Doe *et al*., 2009). Since electroosmotic flow is a surface driven phenomena, v_{eo} is largely independent of channel size (outside the limit of double layer overlap). Thus, it tends to be more suitable for operation of nano-fluidic devices than traditional transport mechanisms. Additionally, the ability to perform precise, picoliter scale fluidic handling simply through the manipulation of externally applied voltages significantly simplifies device operation.

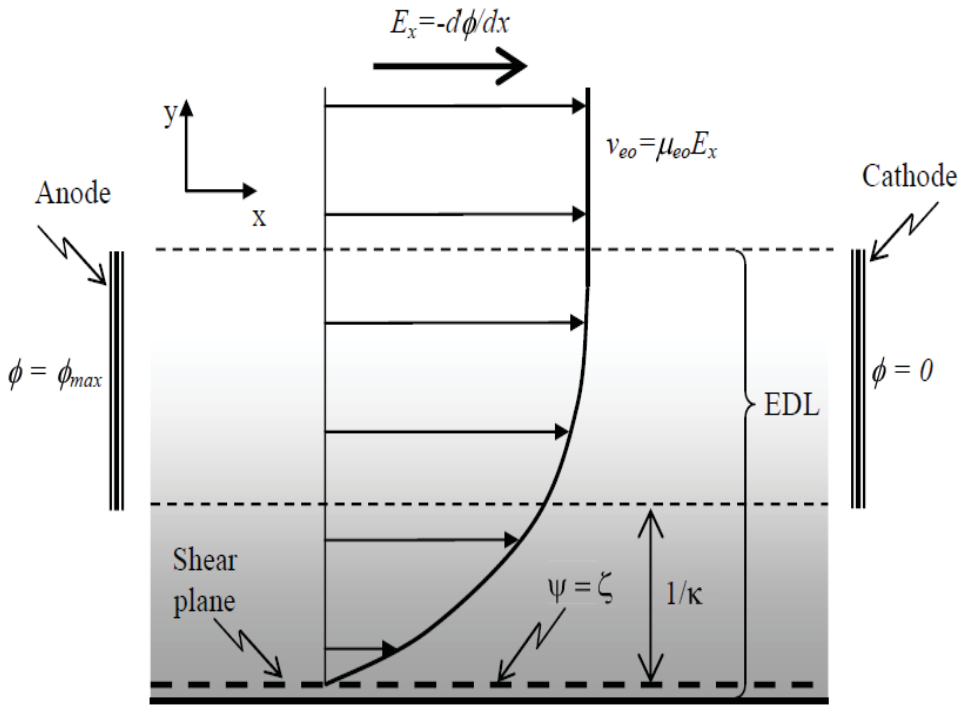

Figure 1.2 Schematic Figure of Electric Double layer showing the exponential decay of diffuse layer (Doe *et al*., 2009)

1.5 Modeling of electrokinetic flow

Electrokinetic flow deals with electro-osmosis and electrophoresis. these are governed by physics of fluid flow and physics of analyte mass transport, thus modeling mathematically and using computational solver of COMSOL Multiphysics Software. A number of authors have made contributions in the area of electrokinetic flow and these are acknowledged as follows.

The field effect regulation of the DNA translocation through a nanopore was investigated using a continuum model, composed of the coupled Poisson-Nernst-Planck equations and Navier-Stokes equation (Jing and Qian *et al*., 2010). The simulation of DNA chip results

in one paper showed that appropriate selection of the analysis point and the design of microchannel structure are important to bring out the diffusion and inertial force effects suitably and increase the sensitivity of the detection of DNA hybridization, that is, the analytical performance of the microfluidic DNA chip (Yamaguchi *et al*., 2005). The equations governing electrokinetic reacting flow were presented together with classical one-dimensional cases that were directly relevant to the flows in electrokinetic devices (MacInnese *et al*., 2002).

In order to overcome the problem of transport of the liquid samples and other solutions in the chip, which are very small dimensions in these Lab-on-chip devices, different methods have been applied. An alternative method of transporting fluid in the samples is through electrokinetic effects, where charged ions in the solutions are subjected to an electric field.

1.6 Analysis of electrokinetic flow

Using the computational solver of COMSOL Multiphysics Software, microfluidic chip models A through E were designed, and simulated for electroosmosis and electrophoretic motion of sample analytes in aqueous solution. Parametric study of electrokinetic flow comprising electro-osmosis and electrophoresis includes the effect of potential difference, zeta potential, current on the concentration distribution and the sample analytes propelling velocity. This parametric study is very useful for modeling and customizing of the ionic fluid flow parameters for analysis of sample analytes. Optimization of the parameters including the microchannel shape, size, injection chamber and analysis

chamber contribute in developing an efficient and effective lab on chip to perform common laboratory procedures.

1.7 T-Shaped microfluidic chip

T-shaped micro-fluidic chip has been widely used for detection, mixing and pumping of analytes samples. T-shaped mixers have been applied in various lab-on-a-chip devices, for example, to dilute sample in a buffer solution (Harrison *et al*., 1993) and to generate concentration gradients (Dertinger *et al*., 2001). Furthermore, Jacobson *et al*. proposed an electroosmotic-based microfluidic device designed with series T-intersections capable of multiple samples parallel mixing. T-shaped microfluidic chip, in this research, was design in such a way that one inlet could be fed with analytes sample and the other with buffer solution so that mixing, pumping and detection could be performed in outlet section.

1.8 Objectives of thesis

The thesis work aims at manipulating velocities and concentration distributions of sample analytes by optimizing parameters such as microchannel size, shape, zeta potential values and electric potential differences between inlets and an outlet in the microfluidic chips.

The specific objectives of this research are as follows:

a) To obtain maximum ionic velocity at the analysis chamber of the microfluidic chips for facilitating the effective electrokinetically driven flow of the analytes.
b) To achieve maximum species accumulation i.e. high concentration of species at the outlet of microfluidic chip for making detectable range of species concentration.

1.9 Organization of thesis

The materials presented in this thesis are organized in a manner that starts with an introduction to the thesis topic in this **Chapter 1**. Modeling of electrokinetic flow in microfluidic chip models using COMSOL Multiphysics software and other literature study are discussed in **Chapter 2** including the solver validation for COMSOL Multiphysics software. **Chapter 3** and **Chapter 4** consist of two major studies, electroosmotic flow and electrophoresis flow respectively, related with electrokinetic flows in microfluidic chips.

Chapter 3 discusses about the ionic velocity in the microfluidic chip due to electroosmosis process in different microfluidic models. **Chapter 4** discusses about the ionic concentration in the microfluidic chip due to electrophoresis process in different microfluidic models with varying electric potentials, zeta potential and mass transport modes. Finally, **Chapter 5** reveals the overall conclusions of the entire thesis and future works associated with electrokinetic flow for the microfluidic chips discussed in this thesis.

CHAPTER 2

MODELING AND VALIDATION OF

ELECTROKINETIC FLOW IN MICROFLUIDIC CHIPS

Microfluidic systems are usually made of various micro-scale structures including microchannels, micro-valves, micro-pumps, etc. To understand the characteristics and phenomenon of electrokinetic driven fluid flow in microchannels, rectangular cross sectioned microchannels with various shapes were studied. Following the geometrical modeling of the microchannels, COMSOL setup is presented in this chapter. Since flow in microchannels only has usually $Re<10$, and in this case $Re<1$, fluid flow in microfluidic systems is assumed to be in very laminar range. Modeling and simulation includes the geometrical modeling of various shapes of microchannels including a T-shaped microfluidic chip and varieties of other modified T-shaped chips.

2.1 Geometrical modeling

A micro-conduit having micro scale dimensions for its height, width and length was selected to study electrokinetic fluid flow by both three dimensional and two dimensional analysis. As shown below in Figure 2.1, a control model of T -shaped microfluidic chip of length 5.25 mm and .25 mm width and height were created in Solid Works, a geometrical software

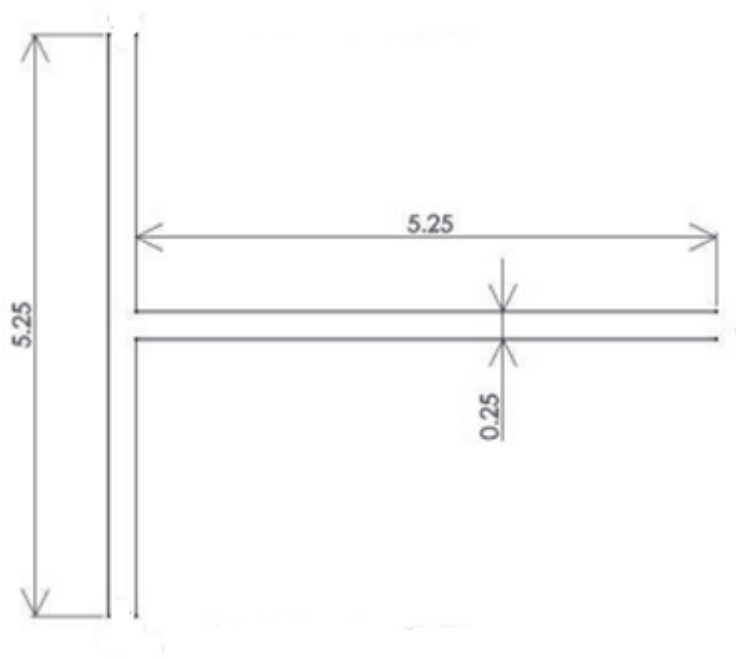

Figure 2.1 Control Model of microfluidic chip (All dimensions are in mm)

2.2 Mathematical modeling

While mathematically modeling the electrically conducting fluid flow in the micro-conduits, multiphysics including physics of fluid flow and physics of ionic mass transport, are coupled together resulting on the effect on propulsion and ionic concentration distribution of the analytes.

The mathematical models consist of a set of governing equations that are used for a closed-form solution and are also embedded within COMSOL 4.2a to analyze and describe the physical phenomena in a given fluid domain. There exist multiple governing equations that each has their own given characteristics to solve for certain values that are based upon the user's interest. The purpose of this chapter is to introduce and describe

the governing equations of the fluid domain. The three equations used are the continuity, momentum, and later developed as the generalized Navier-Stokes equations.

- Incompressible flow – for negligible change in density of fluid flow
- Steady flow – as time dependent analysis is not considered.
- Newtonian fluid - having Newtonian fluid behavior for shear stress generated by fluid motion.

a) Continuity equation

The law of conservation of mass for fluid flow states that the rate of mass leaving a control volume is equal to the rate of mass entering the control volume. In other words, mass is always conserved in a control volume. The statement, expressed mathematically is shown in Equation 2.1 which is further reduced into Equation 2.2.

$$\frac{\partial \rho}{\partial t} + \nabla.(\rho \vec{V}) = 0 \qquad \text{……..……(2.1)}$$

Where, $\frac{\partial \rho}{\partial t} \equiv$ Rate of change of density within the control volume

$\nabla \equiv$ Vector operator in Cartesian coordinates $= \frac{\partial}{\partial x}\hat{i} + \frac{\partial}{\partial y}\hat{j} + \frac{\partial}{\partial z}\hat{k}$

$\nabla.(\rho \vec{V}) \equiv$ Flow across boundaries of the control volume

For incompressible flow, the continuity equation reduces to:

$$\nabla.(\rho \vec{V}) \equiv 0 \qquad \text{…….……(2.2)}$$

b) Navier-Stokes equations

The viscous stresses and the rate of angular deformation, or in other words the rate of shearing strain, are directly proportional to one another for a Newtonian fluid. Since air is considered to be a Newtonian fluid, it is possible to express the viscous stresses in

$$\rho\left(\frac{\partial u}{\partial t}+u\frac{\partial u}{\partial x}+v\frac{\partial u}{\partial y}+w\frac{\partial u}{\partial z}\right)=-\frac{\partial p}{\partial x}+\mu\left(\frac{\partial^2 u}{\partial x^2}+\frac{\partial^2 u}{\partial y^2}+\frac{\partial^2 u}{\partial z^2}\right)+\rho g_x \qquad \text{……..(2.3)}$$

$$\rho\left(\frac{\partial v}{\partial t}+u\frac{\partial v}{\partial x}+v\frac{\partial v}{\partial y}+w\frac{\partial v}{\partial z}\right)=-\frac{\partial p}{\partial y}+\mu\left(\frac{\partial^2 v}{\partial x^2}+\frac{\partial^2 v}{\partial y^2}+\frac{\partial^2 v}{\partial z^2}\right)+\rho g_y \qquad \text{……...(2.4)}$$

$$\rho\left(\frac{\partial w}{\partial t}+u\frac{\partial w}{\partial x}+v\frac{\partial w}{\partial y}+w\frac{\partial w}{\partial z}\right)=-\frac{\partial p}{\partial z}+\mu\left(\frac{\partial^2 w}{\partial x^2}+\frac{\partial^2 w}{\partial y^2}+\frac{\partial^2 w}{\partial z^2}\right)+\rho g_z \qquad \text{……...(2.5)}$$

Taking into account the assumptions stated earlier in this Chapter, the equations can be reduced further. Also, only two-dimensional flow was considered. The simplified Navier-Stokes equations are expressed as Equations 2.6 and 2.7.

$$\rho\left(u\frac{\partial u}{\partial x}+v\frac{\partial u}{\partial y}+w\frac{\partial u}{\partial z}\right)=-\frac{\partial p}{\partial x}+\mu\left(\frac{\partial^2 u}{\partial x^2}+\frac{\partial^2 u}{\partial y^2}+\frac{\partial^2 u}{\partial z^2}\right) \qquad \text{……(2.6)}$$

$$\rho\left(u\frac{\partial v}{\partial x}+v\frac{\partial v}{\partial y}+w\frac{\partial v}{\partial z}\right)=-\frac{\partial p}{\partial y}+\mu\left(\frac{\partial^2 v}{\partial x^2}+\frac{\partial^2 v}{\partial y^2}+\frac{\partial^2 v}{\partial z^2}\right) \qquad \text{……...(2.7)}$$

2.2.1 Problem setup in COMSOL Multiphysics

As shown in Figure 2.2, there are two chambers for inlets whereas an outlet section for analysis chamber. $\mathbf{E_1}$ and $\mathbf{E_2}$ denote the potential difference between two inlets and one outlet. Figures 2.3 to 2.6 show modified T-shaped microfluidic chip meant to be crated for different applications.

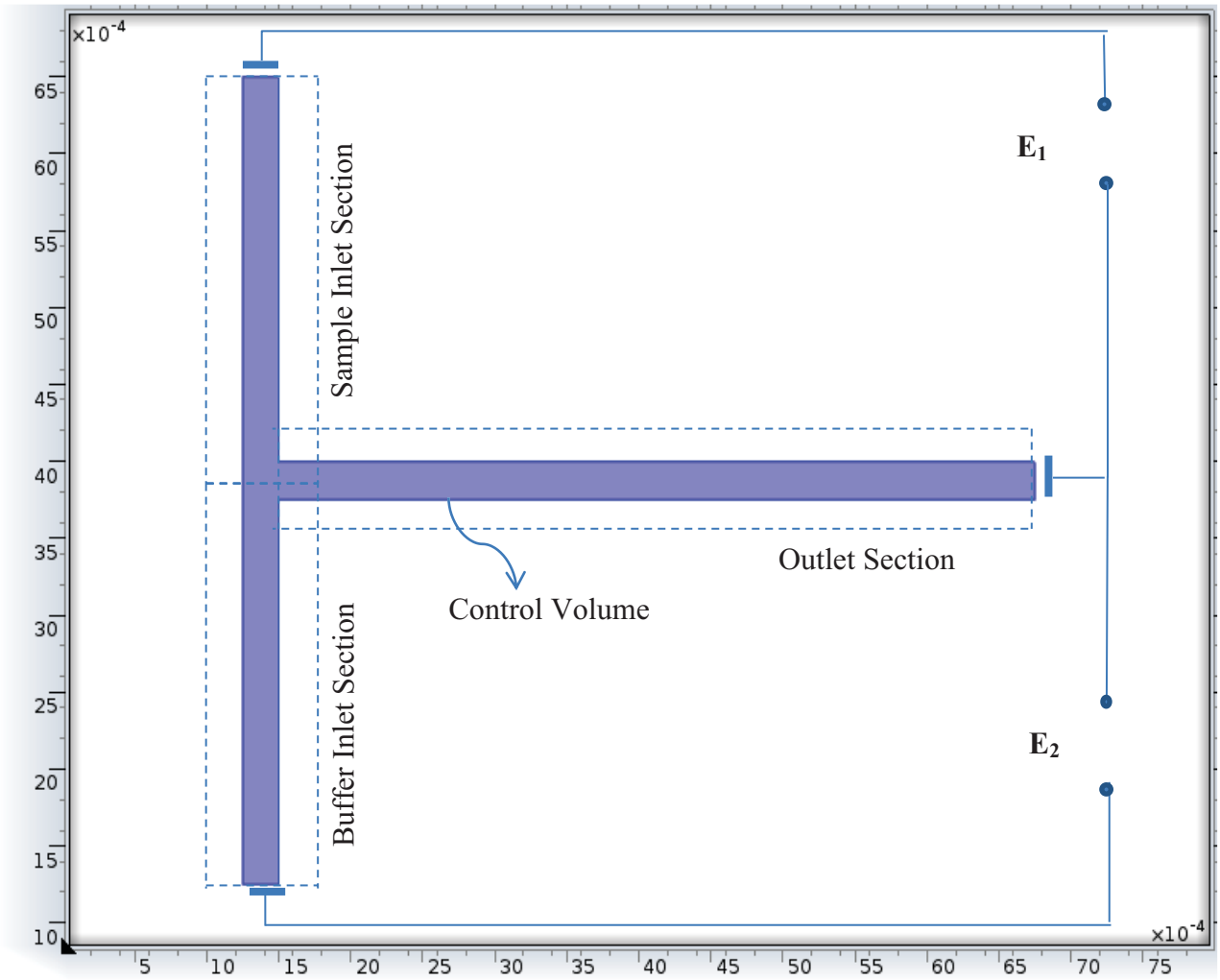

Figure 2.2 Fluid domain of the T-shaped microfluidic chip

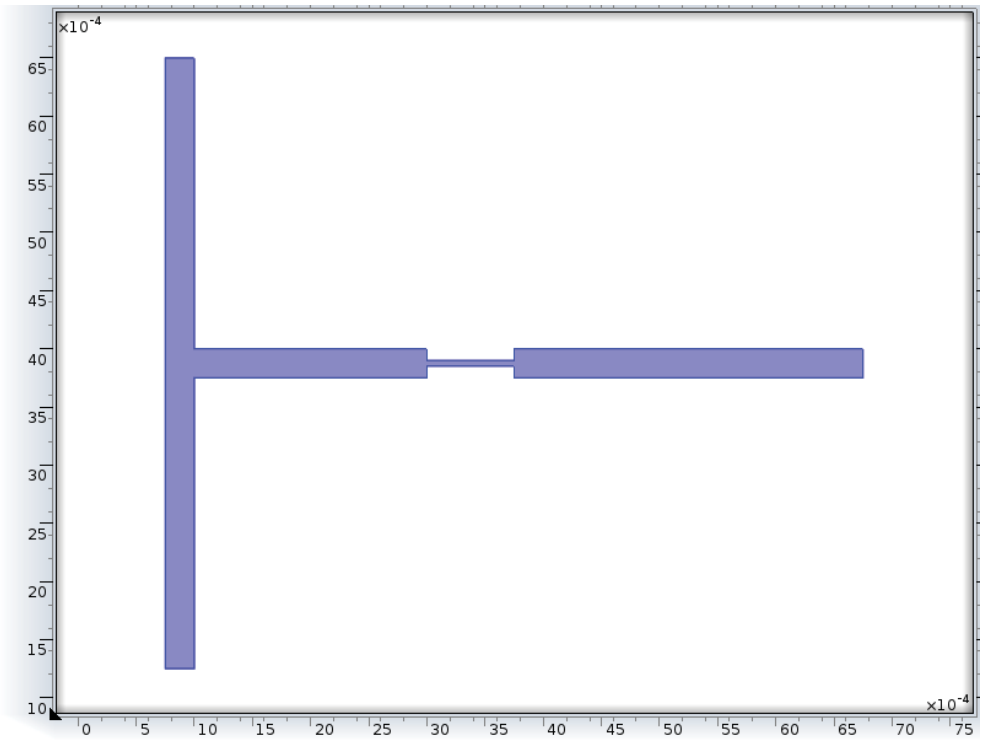

Figure 2.3 Fluid domain of the T-shaped microfluidic chip with a narrowed outlet section

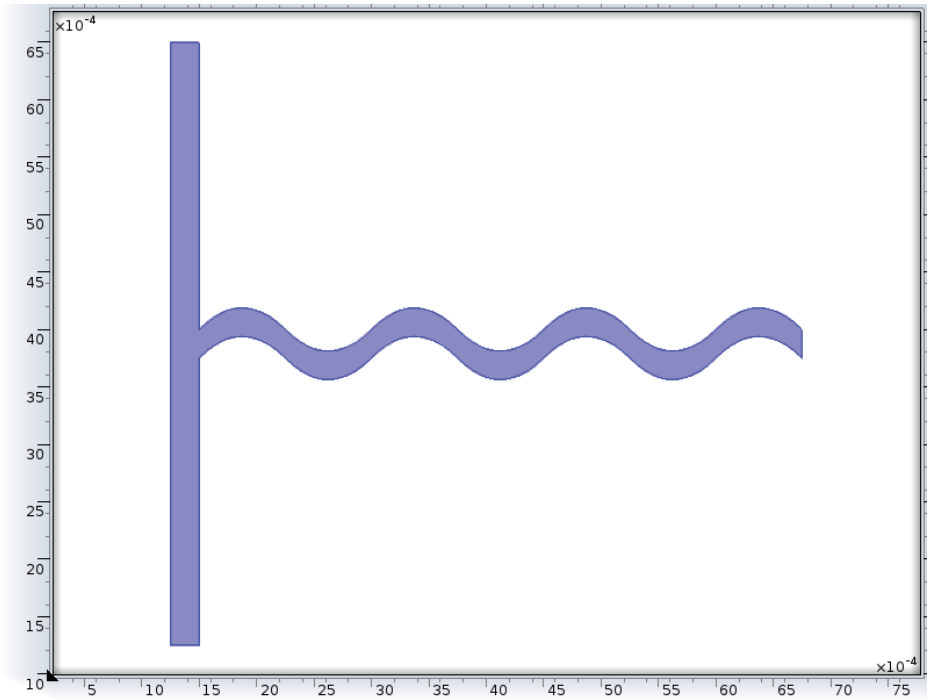

Figure 2.4 Fluid domain of the T-shaped microfluidic chip with a spiral outlet section

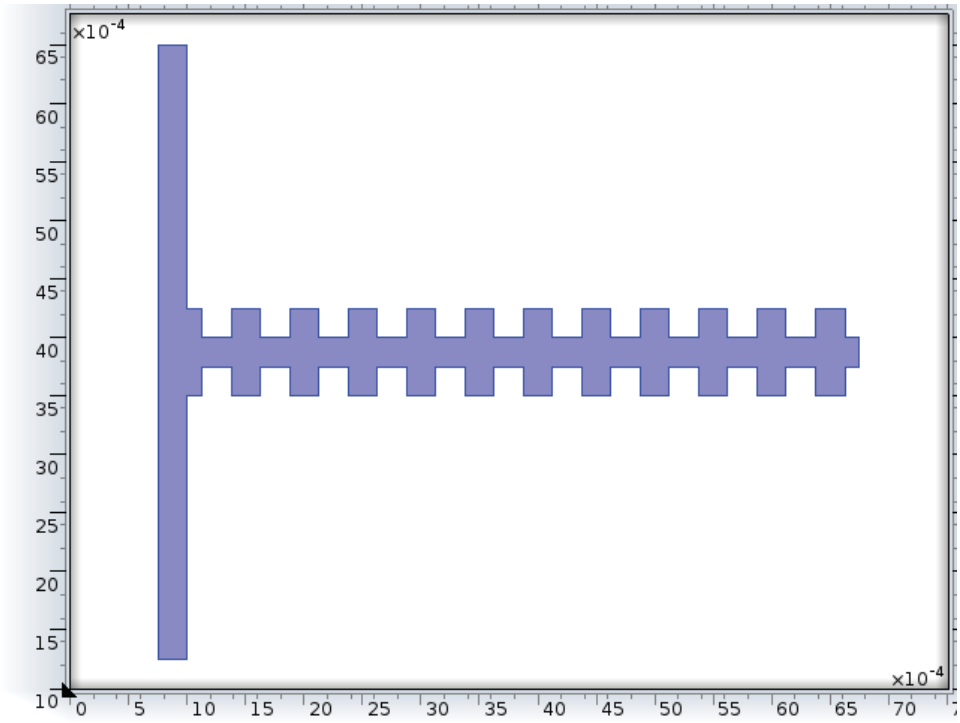

Figure 2.5 Fluid domain of the T-shaped microfluidic chip with a saw tooth outlet section

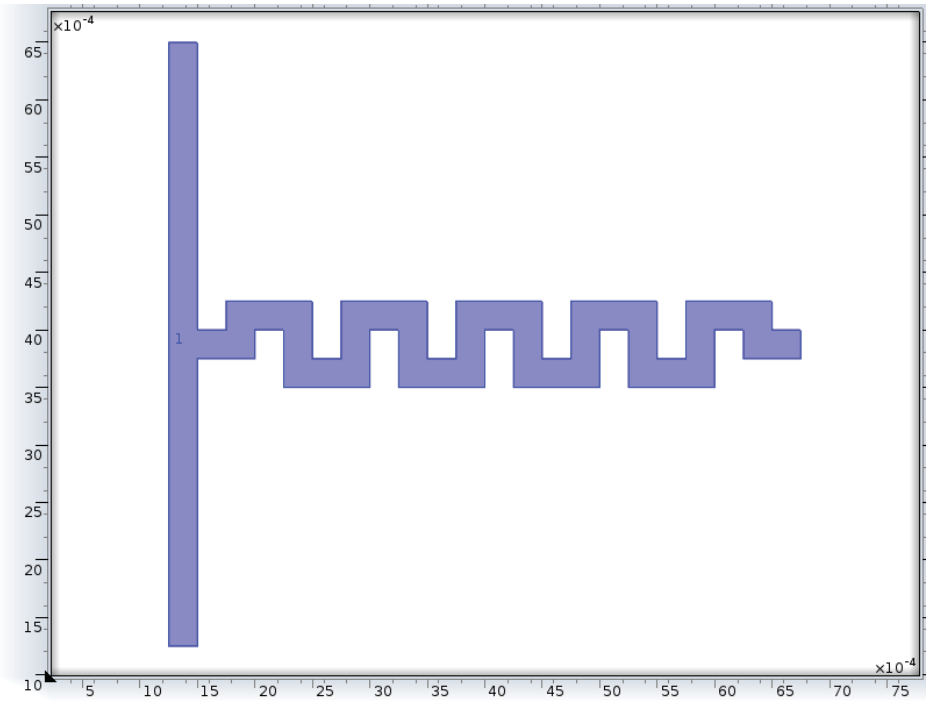

Figure 2.6 Fluid domain of the T-shaped microfluidic chip with a zigzag outlet section

a) Analyte parameters and physical constants

A buffer solution and an analyte solution have to be supplied in the microchannel as shown above. NaCl (Sodium chloride), a very common buffer solution and a targeted analyte has been used for this purpose. Two mechanisms can drive the flow of a saline solution in an electric field: *electro-osmotic flow* and *electrophoretic flow*. Properties of saline solution are shown in Table 2.1.

Table 2.1 Physical constants of sample analyte solution used in microchannels

Rho (ρ)	1000[kg/m^3]	Fluid density
Mu(μ)	1e-3[Pa*s]	Fluid viscosity
D	1e-9[m^2/s]	Sample ion diffusivity
Rg	8.314[J/(mol*K)]	Gas constant
T	298[K]	Fluid temperature
nu	D/(Rg*T)	Sample ion mobility
sigma	1[S/m]	Electric conductivity electrolyte
c_in	0.05*3.5[g/l]/(22+35)[g/mol]	Sample inlet concentration
zeta0(ζ_0)	0.1[V]	Initial Zeta Potential

b) Multi-Physics setup for electroosmotic flow:

- **<u>Physics of fluid flow:</u>**

  Governing equations:

a) Continuity Equation:

$$\nabla \cdot u = 0 \qquad \text{..... (2.8)}$$

b) Navier-Stokes equations

$$\rho\left[\frac{\partial u}{\partial t} + (u.\nabla)u\right] = -\nabla p + \mu\nabla^2 u + \rho_e \mathbf{E} \qquad \text{.....(2.9)}$$

Where, μ denotes the dynamic viscosity (Pa·s), u is the velocity (mm/s), E is the electric field intensity, ρ denotes the fluid's density (kg/m^3), p is the pressure (Pa).

Boundary conditions:

Table 2.2 Boundary conditions for electroosmotic flow used in microchannels

Settings	Sample Inlet	Buffer Inlet	Outlet	Wall
Boundary Condition	Normal Stress	Normal Stress	Pressure, no viscous stress	Electro-osmotic velocity*
P_o			0	
E_x				E_x_emdc
E_y				E_y_emdc
ζ_0				0.1 V
f	0	0		

*Electro-osmotic velocity, $u = \frac{\varepsilon_0 \varepsilon_r \zeta_0}{\eta} \nabla V$

where ε_0 denotes the permittivity of free space (F/m), ε_r is the relative permittivity of water (dimensionless), ζ_0 refers to the zeta potential at the channel wall, and V denotes the potential (V), E_x_emdc and E_y_emdc are electric intensities at x and y-axis respectively.

- **Physics of electrostatics:**

Governing equations:

For Conductive Media DC:

a) Continuity equation:

$$-\nabla . J = Q \qquad \text{……(2.10)}$$

$$J = \sigma E \qquad \text{…..……..(2.11)}$$

b) Elliptic Poisson's equation:

$$-\nabla .(\sigma \nabla V) = Q \qquad \text{……..(2.12)}$$

Where σ denotes conductivity, V is the electric potential, Q refers to a current source and J is current density and E refers to the electric field.

Boundary conditions:

Table 2.3 Boundary conditions for electroosmotic flow used in microchannels

Settings	Sample Inlet	Buffer Inlet	Outlet	Wall
Boundary Type	Electric potential	Electric potential	Electric potential	Electric insulation
V	0	79	120	

c) Multi-Physics setup for electrophoresis

- **Physics of mass transport**

Governing equations:

a) Conservation of ionic mass transport

$$\frac{\partial c}{\partial t} + \nabla.(-D_i \nabla c_i - z_i u_{mi} F c_i \nabla V) = 0 \qquad \text{……..(2.13)}$$

b) Total ionic flux

$$N_i = uc_i - D_i \nabla c_i - z_i m_i F c_i \nabla V \qquad \text{……(2.14)}$$

c) Electro-neutrality

$$\sum_{i=1}^{i} z_i c_i = 0 \qquad \text{……(2.15)}$$

Where, u is the velocity (mm/s), N_k is the flux density, E is the electric field intensity, V denotes the potential (V), c_i is the concentration (mol/m^3), D_i represents the diffusivity

(m^2/s), z_i equals the charge number (which equals 1 for this model), u_{mi} is the mobility (s·mol/kg), and F is Faraday's constant (C/mol).

Boundary conditions:

Table 2.4 Boundary conditions for electrophoretic flow used in microchannels

Settings	Sample Inlet	Buffer Inlet	Outlet	Wall
Boundary Condition	Concentration	Concentration	Convective flux	No Flux
C_o	c_in	0	0	-
N_0	-chds.nmflux_c2	-chds.nmflux_c2	-chds.nmflux_c2	-

Where C_o is concentration (mol/m^3) and N_0 is Net Flux

- **Physics of electrostatics**

Governing equations:

Conductive Media DC:

a) Continuity equation:

$$-\nabla.J = Q \qquad \text{……..……(2.16)}$$

$$J = \sigma E \qquad \text{…….(2.17)}$$

b) Elliptic Poisson's equation:

$$-\nabla.(\sigma \nabla V) = Q \qquad \text{……..(2.18)}$$

Where σ denotes conductivity, V is the electric potential, Q refers to a current source and J is current density and E refers to the electric field.

Boundary conditions:

Table 2.5 Boundary conditions for electrophoretic flow used in microchannels

Settings	Sample Inlet	Buffer Inlet	Outlet	Wall
Boundary Type	Electric potential	Electric potential	Electric potential	Electric insulation
V	-3.5	-3.2	0	0

2.3 Numerical modeling and validation

Numerical analysis involves simulating fluid flow in the micro-conduits through the use of an algorithm and mathematical model. Numerical simulation and modeling allows for these mathematical equations to be solved. Software that combines numerical techniques with the intricacies of fluid flow is utilized. COMSOL 4.2a allows solving a highly complex fluid flow problem with other multiphysics involved. COMSOL Multiphysics is a powerful interactive environment for modeling and solving all kinds of scientific and engineering problems based on partial differential equations (PDEs). This software can easily extend conventional models for one type of physics into multiphysics models that solve coupled physics phenomena—and do so simultaneously. COMSOL Multiphysics then internally compiles a set of PDEs representing the entire model. The meshing schemes depending on the quality of the mesh, enable to achieve varying degrees of accuracy; the finer the mesh, the more accurate the solution. Due to the nature of the problem and the features, a commercially available finite element software COMSOL was used for simulation. The processing and post-processing of the meshed model were performed in COMSOL.

The algorithms and programs that were used in the study of fluid flow and ionic mass transport are discussed in the sections that follow. COMSOL 4.2a couples the equations of flow theory with mathematical models in order to solve highly complex fluid flows. COMSOL Multiphysics includes a number of different solvers for PDE-based problems. Table 2.6 summarizes the available types.

Table 2.6 COMSOL Multiphysics solver types and their usage

Solver Types	**Usage**
Stationary	For stationary PDE problems (linear or nonlinear)
Time-dependent	For time-dependent PDE problems (linear or nonlinear)
Eigen value	For eigenvalue PDE problems
Parametric	For parameterized sets of stationary PDE problems (linear or nonlinear)
Stationary segregated	For stationary multiphysics PDE problems (linear or nonlinear)
Parametric segregated	For parameterized sets of stationary multiphysics PDE problems (linear or nonlinear)
Adaptive	For stationary (linear or nonlinear) or eigenvalue PDE problems using adaptive mesh refinement

The Stationary Segregated Solver is used to solve the microfluidic flow. The solver will be discussed in **Multiphysics methodology.**

2.3.1 Multiphysics methodology

Computational fluid dynamics (CFD) numerical analysis involving multiphysics requires a creation of finite element grids. The general procedures include geometrical drawing, subdomain setting, boundary set up, meshing, simulation and result post processing.

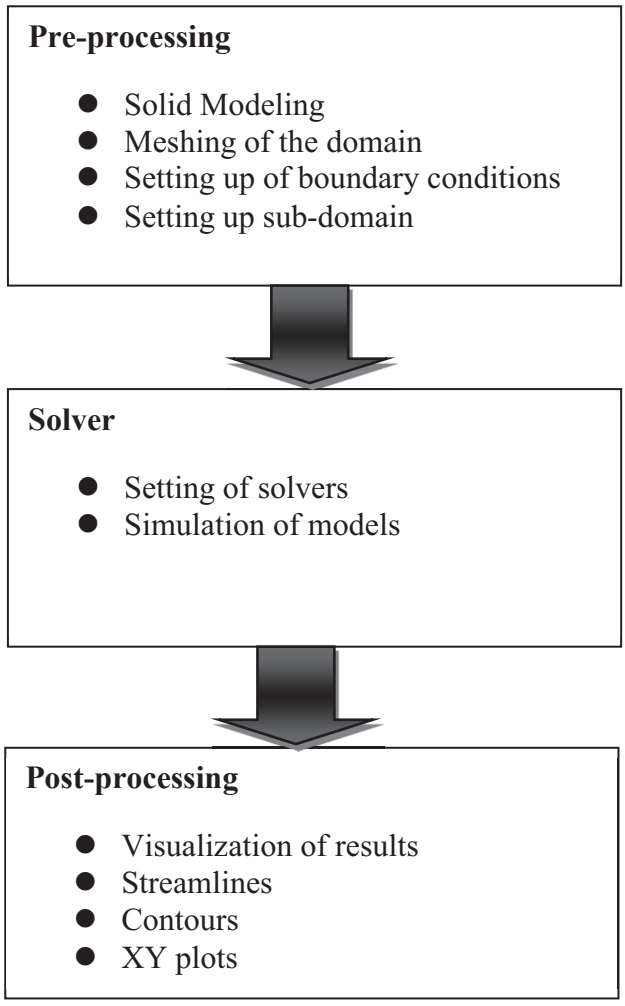

Figure 2.7 Basic program structure of numerical simulation in COMSOL 4.2a

COMSOL 4.2a was used to perform all the required steps from creating models to post processing as shown in Figure 2.7 above and explained below:

1. Construction of the geometrical models using COMSOL 4.2a 2D and 3D drawing with two different modules: Nernst-Plank from Chemical Engineering Module for mass transport modeling and Incompressible Navier-Stokes for fluid flow modeling was used.
2. Division of the fluid domain of the geometrical model into discrete volumes using appropriate meshing parameters. In COMSOL 4.2a, 3D mesh generator was used with tetrahedral, hexahedral, or prism mesh elements whose faces, edges, and corners are called mesh faces, mesh edges, and mesh vertices, respectively. 3D mesh generator includes various shapes of mesh elements. The geometrical boundaries of the model are also automatically partitioned into triangular or quadrilateral boundary elements. The geometric edges are partitioned into edge elements. Isolated geometric vertices become mesh vertices. The free mesher is allows for all types of geometry regardless of the topology and shape of geometry. Boundary conditions define the interface between the model geometry and its surroundings. The subdomain setting describes the physics on a model's main domain, which may be divided into a number of subdomains. The Navier-stokes equations describe laminar flow of viscous fluids through continuity and momentum equations for each respective component of the momentum vector in all spatial dimensions. The Nernst–Planck equation is a conservation of mass equation used to describe the motion of chemical species in a fluid medium. It describes the flux of ions under the influence of both an ionic concentration gradient and an electric field.

3. Before the simulation is begun, the solver parameters setting must be completed. In analysis type's task, we chose Stationary solver for both flow and mass transport physics. The linear system solver is chosen as Direct (PARDISO) for its highly efficient direct solver for both symmetric and nonsymmetrical systems.
4. To help you analyze results from its solvers, COMSOL Multiphysics provides numerous post processing and visualization tools, including advanced graphics, data display and export functions, and a report generator.

The selection of the solver is very important for more accurate results when compared with experimental results and for fewer errors. The user must specify the type of solver, pressure or density based, and whether the flow is steady or unsteady.

The fluid flow was considered as a steady state flow in order to simplify the CFD simulations for the microfluids flow. The stationary solver will be discussed in the following.

(a) Stationary segregated algorithm

Use the stationary segregated solver for linear or nonlinear stationary PDE problems to split the solution steps into substeps. Define the different substeps by grouping solution components' names together. In a solution step for a substep, the segregated solver uses the damped Newton method and computes only the Jacobian related to the solution components, a procedure that can save both memory and assembly time. Also, it is possible to choose which linear system solver to use in a substep independently from other substeps. For problems where a full Newton approach does not converge, a segregated solution approach can sometimes work well. On the other hand, in the vicinity of a solution

where the Newton approach converges quadratically, the segregated solver approach often converges more slowly.

For the segregated solver there is a possibility to directly—that is, without any regards to the equations—impose a restriction on the degrees of freedoms. To use this feature, edit the value of freedom edit field and enter a space-separated list whose entries alternate between component names (the names of the degrees of freedom) and limiting values, for example c1 0 c2 1e-3. For these pairs, the solution vector is modified after each substep in such a way that

$$U_j = \max(U_j, U^L) \qquad \text{..... (2.19)}$$

Where, Uj's are the corresponding degrees if freedoms and U^L denotes the limiting value. Note that if either Uj or U^L is complex valued the real part of that quantity is used in the above equation.

(b) PARDISO direct solver

The parallel sparse direct linear solver PARDISO works on general systems of the form Ax = b. In order to improve sequential and parallel sparse numerical factorization performance, the solver algorithms are based on a Level-3 BLAS update, and they exploit pipelining parallelism with a combination of left-looking and right-looking supernode techniques. The code is written in C and Fortran. COMSOL Multiphysics uses the PARDISO version developed by Olaf Schenk and collaborators, which is included with Intel MKL (Intel Math Kernel Library).

In the Linear System Solver Settings dialog box, following preordering algorithms can be chosen:

- Minimum degree
- Nested dissection (the default algorithm)

It can also specify if the solver should use a maximum weight matching strategy by choosing row preordering on (default) or off. For symmetric matrices there is a choice between using 2-by-2 Bunch-Kaufmann pivoting (default) or not. In the case of positive definite matrices, row preordering and 2-by-2 Bunch-Kaufmann pivoting are not needed. The solution time is usually reduced if you deselect these features.

To avoid pivoting, PARDISO uses a pivot perturbation strategy that tests the magnitude of the potential pivot against a constant threshold of

$$\varepsilon = \alpha \left| PP_{\mathrm{MPS}} D_r A D_c P \right|_{\infty} \qquad \text{.....(2.20)}$$

Where P and PMPS are permutation matrices, Dr and Dc are diagonal scaling matrices, and is the infinity norm (maximum norm). If the solver encounters a tiny pivot during elimination, it sets it to

$$\mathrm{sign}(l_{ii})\varepsilon \left| PP_{\mathrm{MPS}} D_r A D_c P \right|_{\infty} \qquad \text{.....(2.21)}$$

The pivot threshold ε can be specified as required. The perturbation strategy is not as robust as ordinary pivoting. In order to improve the solution PARDISO uses iterative refinements. PARDISO also includes out-of-core capabilities. The PARDISO out-of-core solver stores the LU factors on the hard drive. This minimizes the internal memory usage. The price is longer solution times because it takes longer time to read and write to disk than using the internal memory. You can specify the temporary directory where PARDISO

stores the LU factors using the -tmpdir switch; see page 53 of the COMSOL 4.2a Multiphysics Installation and Operations Guide for further details. The LU factors are stored as blocks on the hard drive. The In core memory option controls the maximum amount of internal memory (in megabytes) allowed for the blocks. If a block is too large to fit into the maximum allowed internal memory you get an out-of-memory error. In that case you must increase the amount of internal memory that you enter in the In core memory edit field. The default value is 512 MB.

COMSOL 4.2a Multiphysics can optionally estimate and check the error after the solution phase. You control this option through the Check tolerances list. For the Automatic selection, error checking is at least done for problems where pivot perturbation or iterative improvement has been used.

(c) Convergence criteria

The segregated solver terminates if a convergence criterion is fulfilled or if the number of segregated iterations exceeds the number in the Maximum number of segregated iterations edit field (in the Stationary page settings). The value in the Tolerance (default = 10−3) edit field for each group in the General page settings gives the convergence criterion. The segregated-solver iterations stop when for all groups the relative error estimate is smaller than the corresponding tolerance.

When termination of the segregated solver is based on the estimated error, it terminates if, for all the group's j, the error estimate is smaller than the corresponding tolerance,

$$\mathrm{err}_{j,k} < \mathrm{tol}_j, \qquad \text{.....(2.22)}$$

Where, the error estimate in segregated iteration k is

$$\mathrm{err}_{j,k} = \max(e^{N}_{j,k}, e^{S}_{j,k}) \qquad \text{.....(2.23)}$$

The number tol_j is taken from the Relative tolerance edit field for the corresponding group settings for the Stationary segregated solver on the General page of the Solver Parameters dialog box. Furthermore,

$$e^{N}_{j,k} = \max_l(1-\alpha_l)\left[\frac{1}{N_j}\sum_{i=1}^{N_j}\left(\frac{\left|(\Delta U^{l,j,k})_i\right|}{W^j_i}\right)^2\right]^{1/2} \qquad \text{.....(2.24)}$$

This is an estimate of the largest damped Newton error. Here l is taken for all iterations in all substeps solving for the group j, αl is the damping factor, ΔU l, j, k is the Newton increment vector, and Nj is the number of DOFs. The weight factor Wji is described below.

$$e^{S}_{j,k} = \left[\frac{1}{N_j}\sum_{i=1}^{N_j}\left(\frac{\left|(U^{j,k}-U^{j,k-1})_i\right|}{W^j_i}\right)^2\right]^{1/2} \qquad \text{.....(2.25)}$$

Where, $e^{S}_{j,k}$ is the relative increment over one complete iteration k. In this expression, Uj,k is the segregated solution vector for the group j, and Wji = max(|Uji|, Si), where Si is a scale factor that the solver determines from the settings in the Scaling of variables area.

The selection in the Matrix symmetry list applies to all the segregated solver groups. For the Automatic choice, the solver can detect and make use of symmetry for the group Jacobian independently of other groups.

The selection in the Linearity list on the Stationary page applies to all the segregated solver groups. This selection is not as important as it is for the standard stationary solver because the stationary segregated solver uses the same iterative procedure both for linear and

nonlinear problems and always checks the error criteria. The associated settings do affect which group Jacobians that are reassembled, and an incorrect selection can therefore result in suboptimal convergence.

2.3.2 Solver validation

To numerically solve the strongly coupled two and three dimensional microfluidic systems, the commercially available finite element software package COMSOL_version 4.2a, (www.comsol.com) operating with a 64 bit dual-processor workstation of 32 GB RAM was used. The 2D and 3D computational domains were discretized into quadratic triangular elements. Non-uniform elements with a larger number of elements next to the inlet and outlet cross sections, as well as along the surfaces of the channel walls were employed where the electrochemical reactions occur. Solutions obtained for different mesh sizes were compared to ensure that the numerical solutions are convergent, independent of the size of the finite elements, and satisfy the governing laws for fluid flow and chemical mass transport. To verify the code, the numerical predictions with solutions available in the literature for special cases such as an electrochemical reactor with known flow field and the two-dimensional electrokinetic flow in the presence of abundant saline solution were compared and validated. Simulation of the 2D parallel-plate electrochemical reactor described in Georgiadou (2003) was compared with similar model to the configuration depicted in Figure 2.10. The computational domain consists of an upstream region, a downstream region, and the region between two parallel electrode surfaces positioned along the opposing walls. In contrast to the microfluidic channel as described in this work, in the PPER reactor, a parabolic flow field is specified. In other

words, one only needs to solve the Nernst-Planck equations using the prescribed velocity profile and electroneutrality. Simulation results are found in excellent agreement with the finite difference results of Georgiadou. COMSOL numerical solution favorably agrees with the analytical solution mentioned above (results are not shown here). COMSOL numerical solution favorably agrees with the analytical solution presented by Kabbani *et al* (2007). The good agreement of our computational results with the results obtained with different computational techniques as well as other comparisons with specialized solutions for the electrokinetic flow give us confidence in our COMSOL computational results. This thesis work requires COMSOL solver validation for mixing, pumping, concentration profiles due to electrokinetic flow in microfluidic chips including electro-osmosis and electrophoresis effects. Solver validation for such processes are presented below:

(a) Solver validation for mixing

(b) Solver Validation for pumping

(c) Solver validation for concentration

(d) Solver validation for electrokinetic flow

a) Solver validation for mixing

A review was made on mixing process in regard to mass fractions at different velocities of various mixers when the fluids contact each other (Panta *et al.,* 2011). The qualitative validation of the numerical simulations was based on the numerical simulation results from Micro T-mixer as a rapid mixing micromixer by Seck Hoe Wong, Michael C.L. Ward and Christopher W. Wharton. Similar model (as shown in Figure 2.8) was drawn

and simulated on ANSYS/Fluent software (that uses the cell-centered (CC) finite volume approach) and results were compared for validation. The results obtained had 22% error in terms of Reynolds number from the results of referred work.

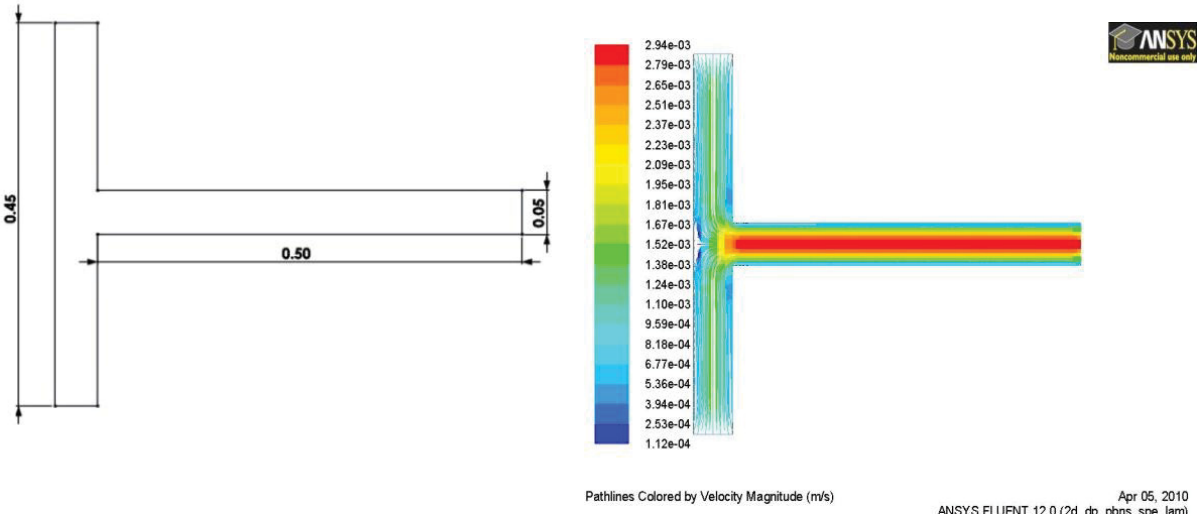

Figure 2.8 Velocity of flow in a T-micromixer for inlet velocity = 0.001m/s.

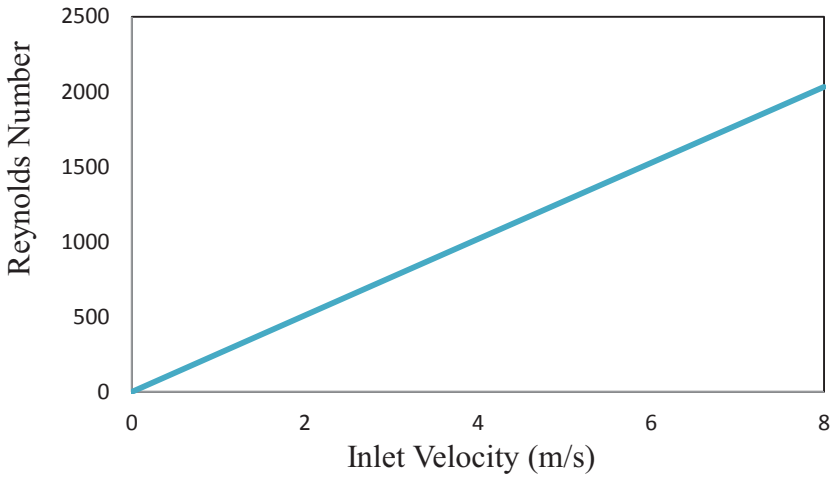

Figure 2.9 Reynolds number Vs. inlet velocity (m/s) T-micromixer

b) Solver validation for pumping

Microchannels were designed and modeled to run 3D fluid flow simulation for MHD (Magneto-hydrodyanmics) investigation (Panta *et al.,* 2010). Rectangular microchannels' geometries in the order of micrometers were created, preprocessed, simulated and post processed in COMSOL, commercially available finite element software. In order to validate the simulation results, the problem set up in COMSOL 3.5a were made same as those used in the experiments (Aguilar *et al.,* 2006). The average velocities obtained from the 3D model and experimental data taken from the literature were compared and validated as shown in figure below. In addition, the simulation results were compared with the published data (Kabbani *et al.,* 2007) and obtained in a close arrangement.

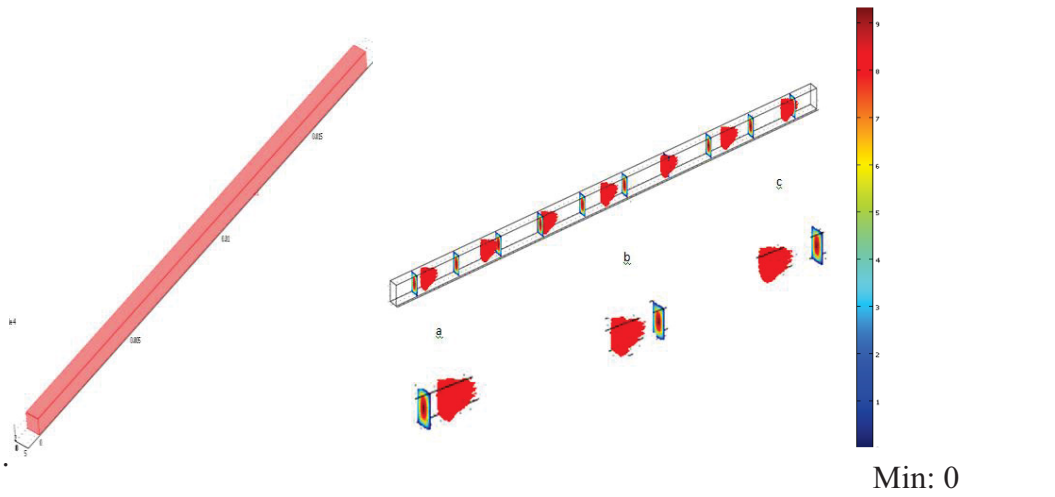

Figure 2.10 Velocity distribution of MHD fluid flow in straight microchannel with the velocity vectors showing the velocity contours at (a) inlet (b) mid-section and (c) outlet respectively. The concentration of the RedOx species ($K_4[Fe(CN)_6]$) /$K_3[Fe(CN)_6]$) C0=0.25 M when the magnetic flux density, B =0.44 T and the =dimensions of the conduit are L=18 mm, W=330 µm, inlet H=670 µm and outlet H=1340 µm.

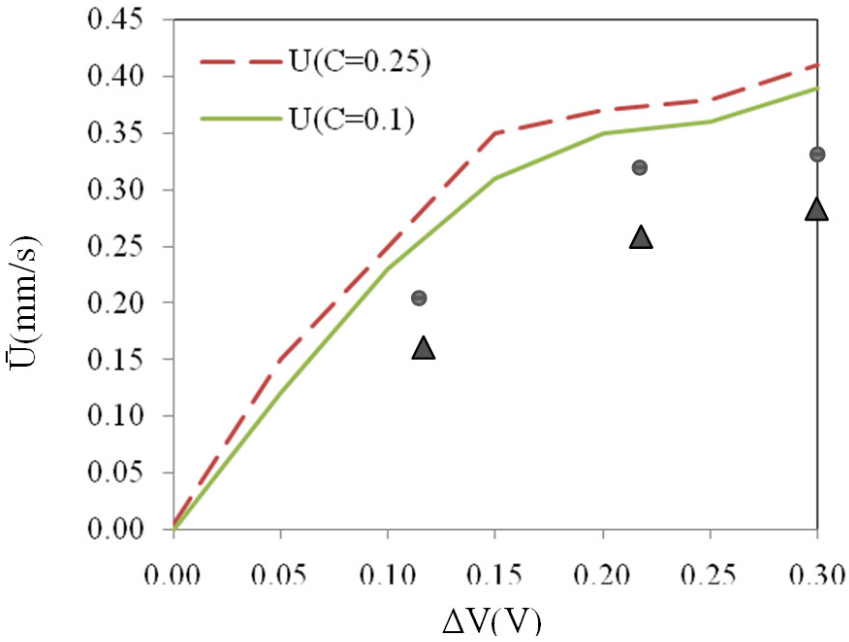

Figure 2.11 Effect of potential difference on the average velocity with various concentration of RedOx species $K_4[Fe(CN)_6]$) /$K_3[Fe(CN)_6]$ Co=0.1 M and Co=0.25 M when B=0.44 T. The triangles (▲) and circles (●) represent the experimental data (*Aguilar et al. 2006)* where the solid and the dashed lines represent, respectively, the results obtained from the 3D model simulations.

c) Solver validation for concentration

Experimental concentration profile with simulated contour lines was compared during sample loading in microchip as shown in Figure 2.12 (Jacobson *et al.,* 2000). Computer modeling results of two injection techniques in the channel cross geometry were used to identify a set of running parameters providing optimal performance. COMSOL was used to find concentration contour in the chip.

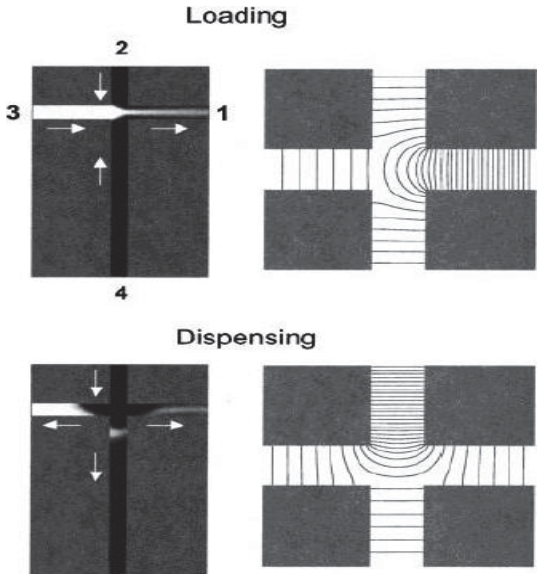

Figure 2.12 Simulated images of the injection sequence for the pinched valve: loading (top); dispensing (bottom). The sample is shown in white with arrows indicating buffer and sample flow direction (left panels). Equipotential lines (right panels) show the electric field distribution in the area close to the channel intersection.

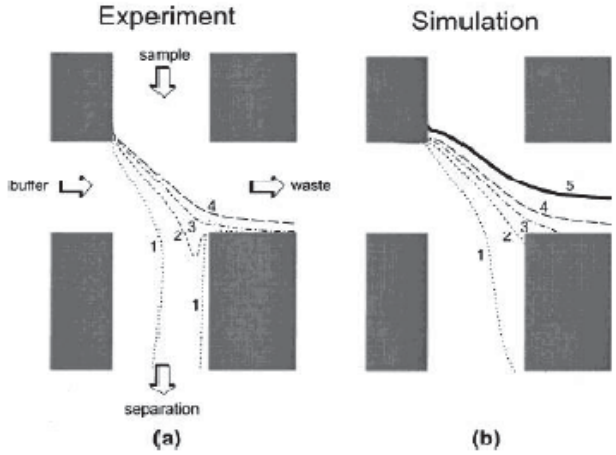

Figure 2.13 Experimental (a) and simulated (b) concentration contour lines during sample loading. Different contour lines correspond to different reference electric fields: (1)E_{max} =38 V/cm, (2) E_{max} =97V/cm, (3)E_{max} =190 V/cm, and (4) E_{max} =380 V/cm, for constant relative electric field strength ε_1 =-0.68, ε_2 =0.42, ε_3 =1.0 and ε_4 =-0.74. Line 5 shows the sample stream boundary in the absenceof diffusion. (Part a reprinted with permission from ref 17, copyright1999 American Chemical Society.)

d) Solver validation for electrokinetic flow

Both two-dimensional and three-dimensional versions of a T- junction as shown in Figure 2.14 were studied (J M. MacInnes, 2002). Both the flows produced by electric potential difference and by pressure difference were computed. The three-dimensional computations showed close similarity to the two-dimensional case for electrokinetic flow, but for pressure flow the three-dimensional flow was significantly changed in relation to the corresponding two-dimensional case.

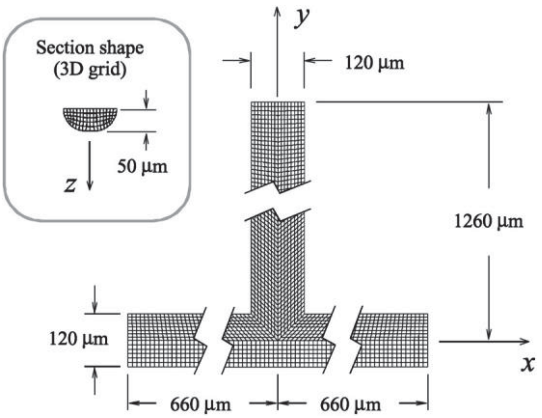

Figure 2.14 Geometry and computational grid of a T-junction chip (*JM MacInnes, 2002*)

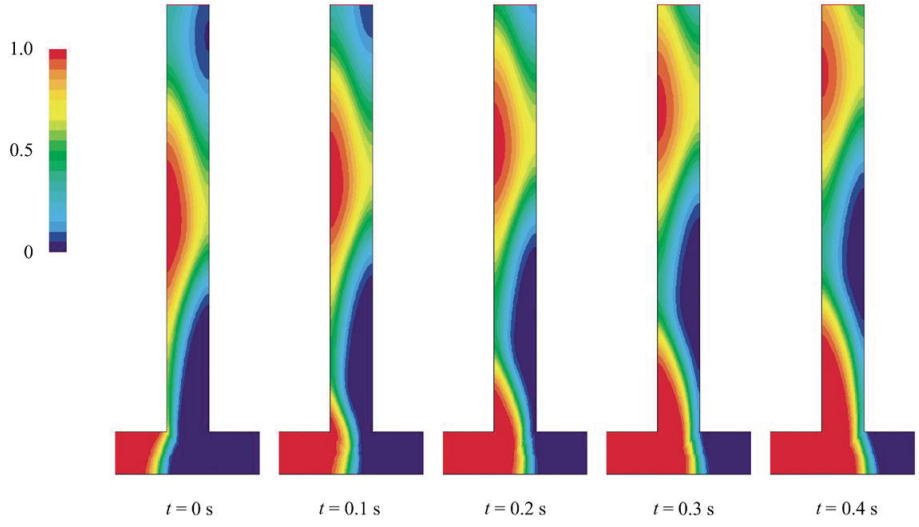

Figure 2.15 Contours of the mass fraction of species due to electrokinetic flow for the T-junction chip (*JM MacInnes, 2002*)

CHAPTER 3

ANALYSIS OF ELECTROOSMOTIC FLOW IN MICROFLUICIC CHIPS*

Lab-on-chip devices promise many novel applications concerning the transport of the liquid samples and buffer solutions on the order of micro-scale dimensions. One of the efficient methods for transporting ionic liquid samples is through electrokinetic effects, where an electric field will be applied to charged ions such as DNA, a negatively charged ion and propel it through a microchannel for its identification and/or detection. These ions, mixed with the aforementioned buffer, solution act as carriers of the entire solution through the selective microchannels supplied from the inlets via the probe region for its detection to the outlet. COMSOL, commercially available multiphysics software, with its specific MEMS and Chemical Engineering modules was employed to model and simulate for the analysis of velocity and concentration of the liquid ionic samples throughout the channel of various shapes. Thus obtained ionic fluid concentrations and velocities were plotted against various modeling parameters such as potential difference across the two inlets, in which analyte sample and buffer solutions were supplied from the two inlets of a typical T-shaped microfluidic chip.

Keywords: Electrokinetic flow, Ionic fluid, COMSOL

*Partial Contents of this chapter was presented at 2011 American Society of Mechanical Engineers Summer Bioengineering (ASME-SBC) conference, Farmington, PA, USA and US National Committee on Biomechanics-3rd Symposium on Frontiers in Biomechanics: Mechanics of Development, June 22-25

3.1 Introduction

Miniaturization and integration technology that have been successfully used in microelectronics and information technology are nowadays adapted also to analytical science, based on miniaturized total analysis system (μTAS) made from microfluidics components (Utsumi *et al.,* 2007). Microfluidics and more recently nanofluidic devices are rapidly emerging miniaturized tools having enormous potentials for a wide range of applications including DNA analysis, drug delivery and proteomic analysis (Postler *et al.,* 2008). Operation of microfluidic devices involves delivering buffer solutions and manipulating mobility of ionic liquid samples by injecting, pumping, mixing, focusing, controlling, separating, etc. (Yang *et al.,* 2009). Electroosmotic, gas-pressure, positive displacement, micro-peristaltic, thermal, micro-hydrodynamic (MHD), etc. have been commonly used to propel the fluid flow in the micro/nano channels (Yamaguchi *et al.,* 2006 and Panta *et al.,* 2008).

A previous study reports the usability of microfluidic chips for detecting DNA hybridization (Yamaguchi *et al.,* 2006). This study also reported the influence of the inertial force exerted on DNA molecules and the diffusion of DNA molecules. The computer simulations showed the appropriate selection of analysis parameters and the design of microchannel structure is crucial for diffusion and inertial forces to increase the sensitivity of the detection of DNA hybridization.

Poisson-Nernst-Planck equations had been used for the ionic mass transport and the Navier-Stokes used for the hydrodynamic field (Qian *et al.,* 2010). Two reservoirs were connected with the nanopore where the DNA is to be transported from one reservoir to

other. The variation of axial velocity at the nanopore under two different applied electric fields was compared in the research (Qian *et al.,* 2010). For generation of electroosmotic forces and for translocation to attract DNA molecules from the inlet reservoir to the nanopore, a positive gate potential was applied. When a positive gate potential is applied, the DNA nanoparticle was attracted into the nanopore much faster, compared to other methods.

In order to transport the liquid ionic samples and buffer solutions in the microchannel, an alternative method of transporting ionic sample solutions is through electrokinetic effects was applied. In electrokinetic fluid propulsion, charged ions in the solution were subjected to an electric field as explained on published work (MacInnes, 2002). Based on a model of microfluidic DNA chips from COMSOL library shown in Figure 3.1 (*http://www.comsol.com*, retrieved on 01/15/11), with two inlets: one for analyte and other for buffer solution supply and an outlet ports was used as the "control model", various shapes of microchaannels were modeled for investigation as depicted in Figure 3.2 (Models B through E).

3.2 Mathematical modeling

Based on the main model used from COMSOL library shown in Figure 3.1, named as "Control Model", charged solution is formed to the wall surfaces during the electrokinetic fluid motion. This layer is referred to as a diffuse layer. The layer is dependent on the material used; and the type of charged groups formed i.e negatively or positively charged groups on the wall's surfaces. The potential difference imposed between its different parts produces a flow in the vertical or horizontal direction, depending on the direction of imposed field. The control model is depicted in Figure 3.1

and the geometry has modified to see the flow variation with the changed geometry. The electric potential differences at the open boundaries between inlets and outlets are applied where fluid is allowed to enter or enter the channel port. The flow is expected to be laminar with of very low Reynolds number (Re<10). In order to justify the elecroosmotic flow the Stokes flow equations could be used. From a published work (MacInnes, 2002), the stokes flow equations are derived from the Navier –Stokes equations assuming that the inertial term is zero. Unlike the Navier-Stokes equations, the Stokes equations form a nearly linear system of equations.

In general, the fluid motion in the microchannel is modeled by the Navier Stokes equation and continuity equation; assuming the fluid is incompressible.

Conservation of mass: Continuity equation

$$\nabla . u = 0 \qquad \text{……(3.1)}$$

Conservation of momentum: Navier Stokes equation

$$\rho\left[\frac{\partial u}{\partial t} + (u.\nabla)u\right] = -\nabla p + \mu\nabla^2 u + \rho_e \mathbf{E} \qquad \text{……(3.2)}$$

Where ρ_e is the charge density (C/m^3), ρ denotes the fluid's density (kg/m^3), **E** is the electric field intensity (V) and μ is the dynamic viscosity (m^2/s) and u is the velocity (mm/s), p is the pressure (Pa)

The slip velocity as shown in Figure 3.1 (c) at the edge of the electric double layer is given by

$$u = \frac{\varepsilon_0 \varepsilon_r \varsigma_0}{\eta} \nabla V \qquad \text{…….……(3.3)}$$

Similarly, ionic concentration of bulk solution in the microchannel is given by:

$$\frac{\partial c}{\partial t} + \nabla.(-D_i \nabla c_i - z_i u_{mi} F c_i \nabla V) = 0 \qquad \text{……..……..……(3.4)}$$

Where, η denotes the dynamic viscosity (Pa·s), **u** is the velocity (mm/s), ε_0 denotes the permittivity of free space (F/m), ε_r is the relative permittivity of water (dimensionless), ζ_0 refers to the zeta potential at the channel wall (V), and V denotes the electric potential (V), c_i is the concentration of $_i$ species (mol/m^3), D_i represents the diffusivity of the sepcies (m^2/s), z_i equals the charge number of i species(which equals 1 for this model), u_{mi} is the mobility of I species (s·mol/kg), and F is Universal Faraday's constant (C/mol).

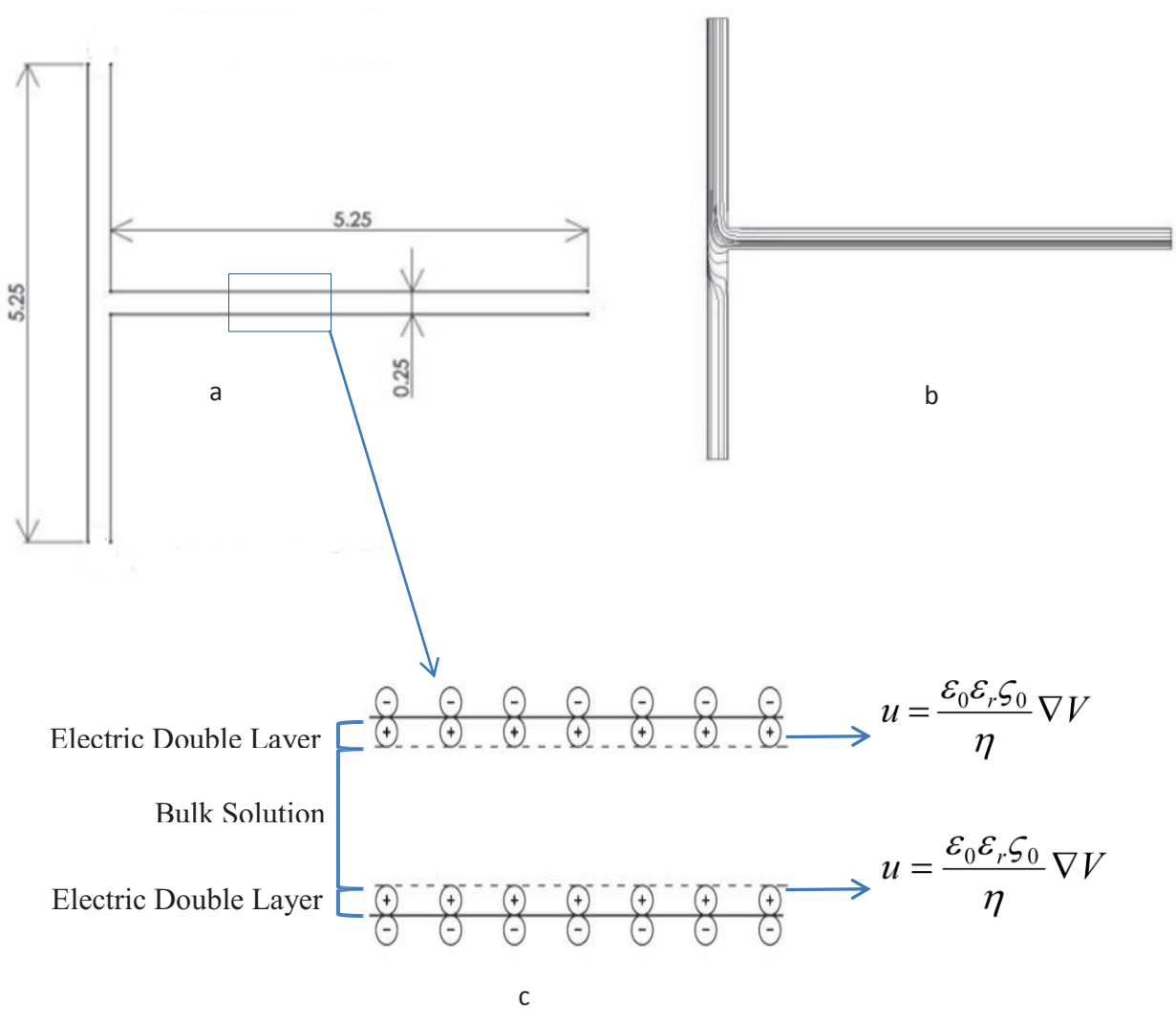

Figure 3.1 a) Microfluidic chip model (All dimensions are in mm), b) streamlines of velocity obtained from COMSOL simulation, c) slip velocity at wall surfaces

3.3 Results and discussions

The T-shaped microfluidic chip model (Control Model) of 0.25 mm width with saline solution supplied through an inlet was modeled. Modeling and simulation was performed using COMSOL. Physics setup including fluid flow and ionic mass transport was applied (MacInnes, 2002). The model was then modified with varying shapes as shown in Figure 3.2. Initially, the two inlets were applied electric potentials of 119 V and 79V across the outlet port in order to measure the maximum electroosmotically driven fluid velocity in the channel. Similarly for mass transport same model was created based on published work (Ramsay et al, 2000) and simulation was done in order to determine the concentration distribution in the outlet section of the chip.

Various potential differences were applied between the two inlet ports that were supplied with analyte solution and the buffer. Similarly, various potential differences were applied at the outlet. Thus designed computer simulation produced the results for the effect of voltage difference on the velocity of analyte solution. Effect of this change in voltage difference on the concentration distribution of the ionic analyte solution is also presented below. Finally, a time dependence or transient analysis in other words has also been discussed.

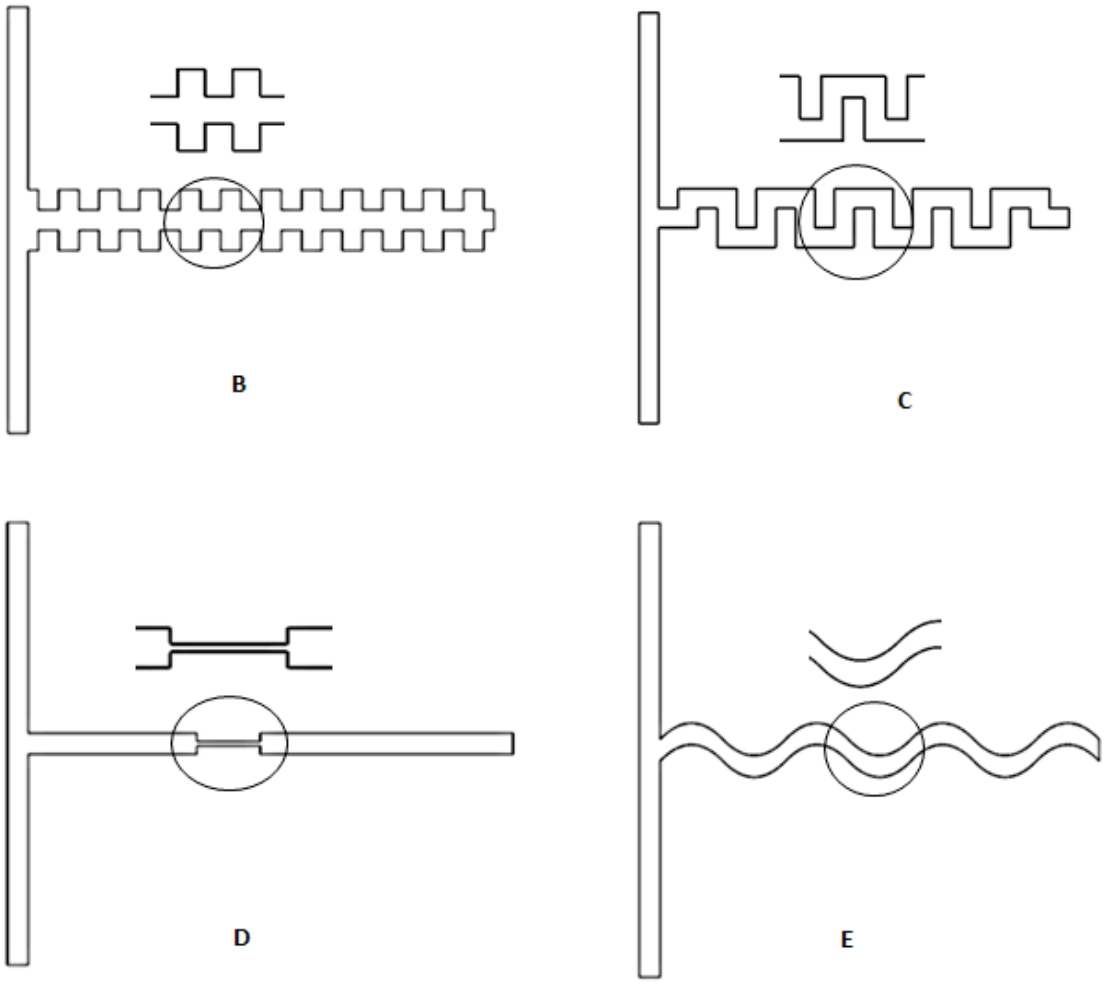

Figure 3.2 Modified geometries of microfluidic chip models (models B, C, D and E)*

*Simulation contours for velocity are shown in **Appendix A.1**

3.3.1 Effect of voltage difference in maximum velocity

The velocity at the outlet section of microchannel decreases with decreasing potential differences. Initially the voltage difference between inlet and outlet was chosen as 119 V as this particular potential difference produced an optimal values of fluid driving motion. Lower velocities were obtained applying the lower voltage differences keeping other parameters constant. Since other parameters are constant, only parameter that effects the formulation of high velocity was potential difference between inlet and the outlet. The maximum velocity was seen in the highlighted part of the model D whereas the velocity obtained for model E was least (Figures 3.3 and 3.4). As shown, the maximum velocity was obtained 1.18 times greater in 3D micro-chip than that obtained from 2D.

For each model, the velocities were found to be decreasing till the voltage difference was applied 20V, and then started to slightly rise as it lowered to 20V. Figure 3.4 illustrates the velocity profiles of fluid in different models plotted against applied potential differences.

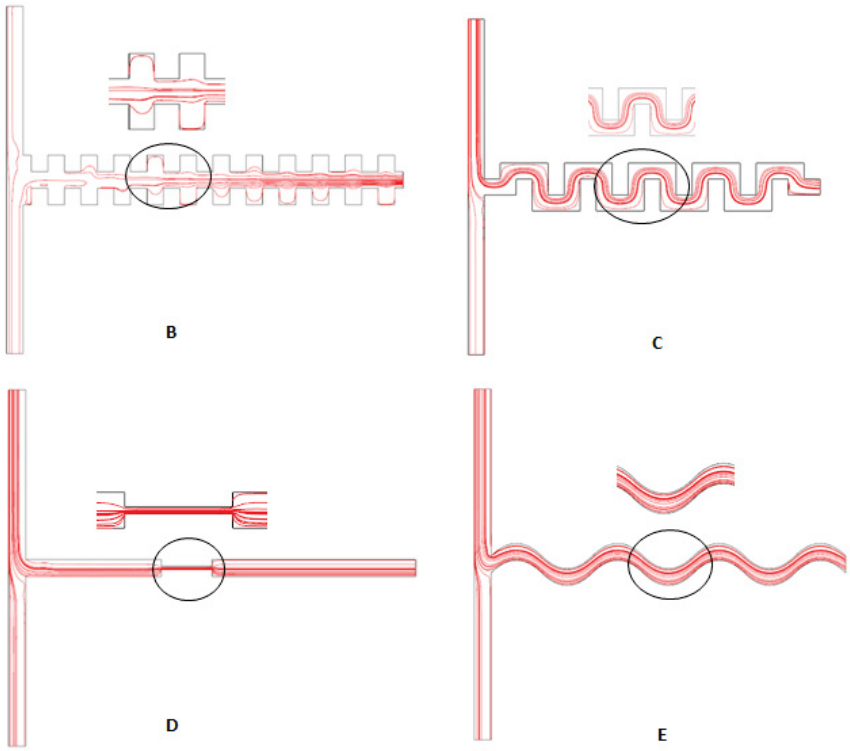

Figure 3.3 Modified geometries of microfluidic chip models showing velocity streamlines field (models B, C, D and E)*

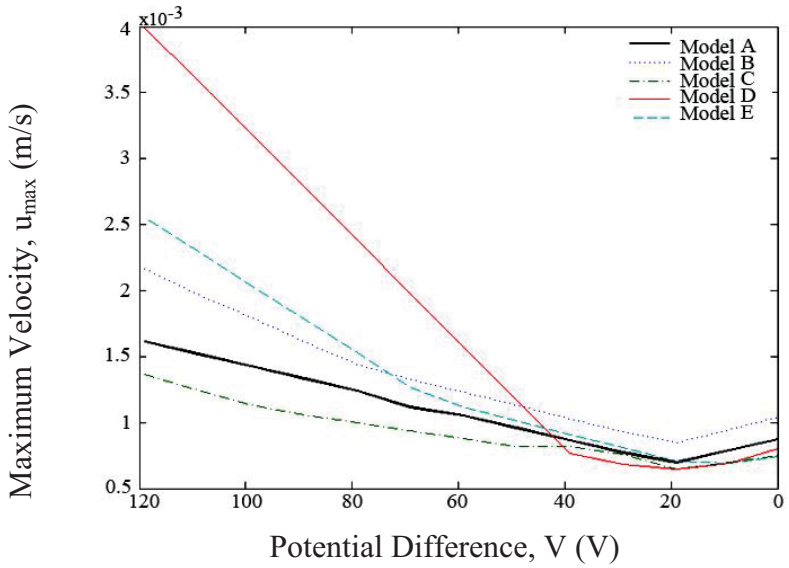

Figure 3.4 Modified geometries of microfluidic chip models showing maximum velocities at any point in the outlet section Vs. potential differences across sample inlet and the outlet (models B, C, D and E compared with model A)

3.3.2 Effect of potential difference in concentration distribution

For the mode of "Conductive media DC" , -1 V and -3.2 V were selected at two inlets vs. outlet, one for sample analyte and one for the buffer solution as done in published work (Ermakov *et al*., 2000). Similarly, for outlet port, 0V was set. For the physics of fluid flow "incompressible Navier-Stokes", electroosmotic velocity was set at the walls of the microchannel and zero pressure at the outlet was prevailed. For mass transport, the mode of "electrokinetic flow" was set with boundary conditions of 3.07 moles per cubic meter of sample analyte at the inlet and zero concentration at another inlet. Also insulation symmetry on the channel, and convective flux at the outlet was set.

Initially, DC voltage of -3V and -1V were imposed at the upper and lower inlets to maintain the concentration distribution at the outlet for -3.2 V upper inlet voltage and -1V lower inlet voltage . As shown in Figure 3.5, lower voltage difference (higher negative voltages) depicts the higher concentrations thus showing the effective mixing for detectable sample concentrations at the outlet region.

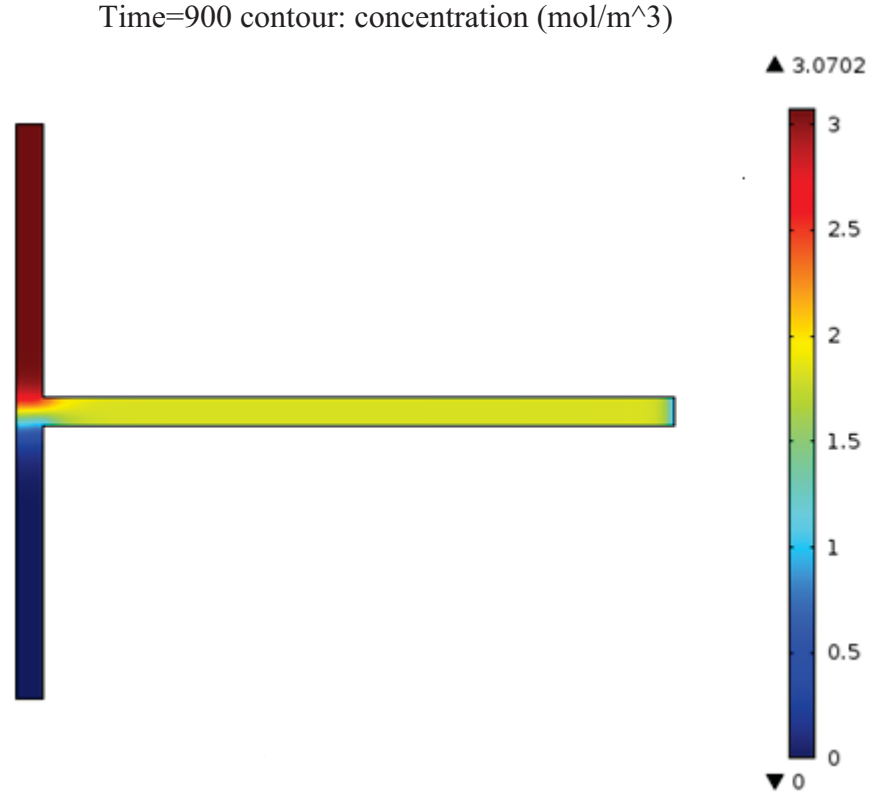

(a)

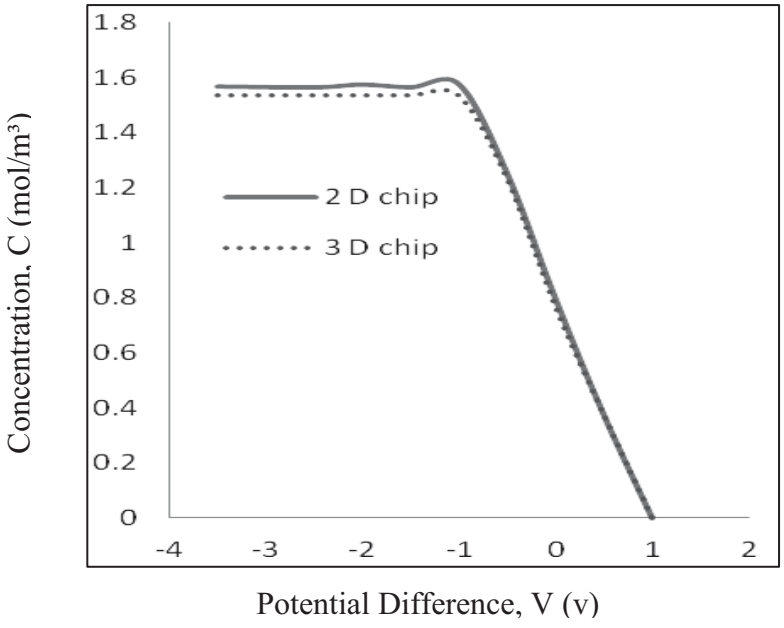

(b)

Figure 3.5 (a) Concentration contour (mol/m³) at time=900 seconds,(b) concentration at the outlet Vs voltage difference between for control model (A)**

3.3.3 Transient analysis in concentration distribution in microfluidic chip

A steady state profile was obtained at approximately 15 minutes after simulation was done. "Electrokinetic flow" was set for the control T-model along with transient boundary conditions to evaluate voltage effect on concentration distributions. To achieve an effective distribution of concentration and confining the sample analytes at detection chamber, simulation was done at various time steps as shown in Figure 3.6.

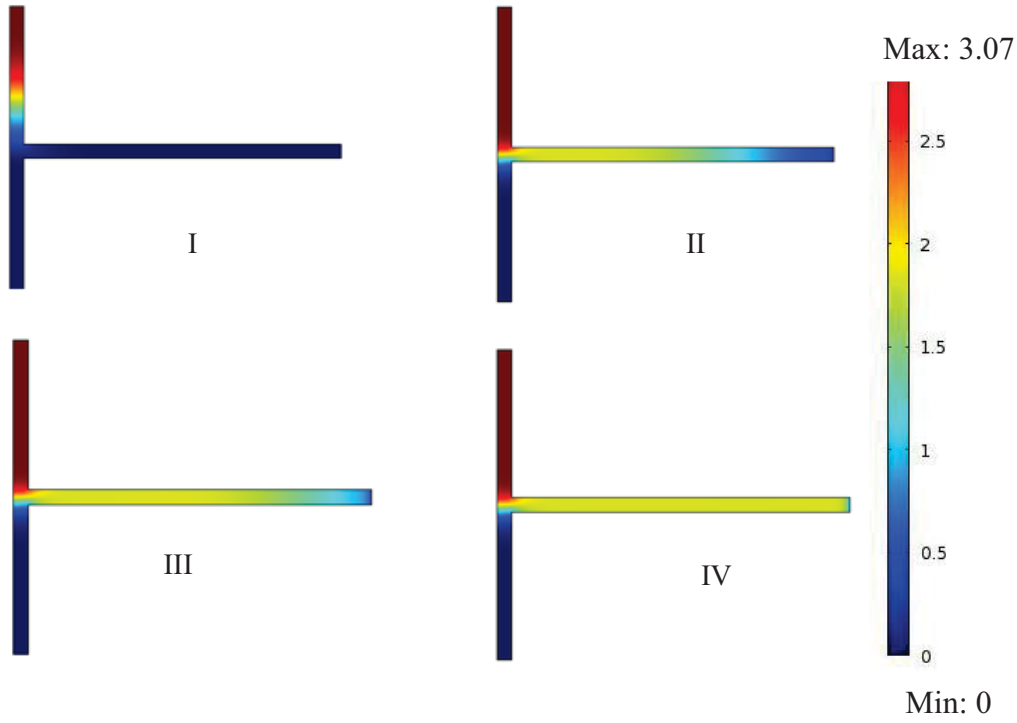

Figure 3.6 Concentration (mol/m³) distributions at different times at 200, 500, 700 and 900 seconds (I, II, III and IV respectively) for the control model**

Figure 3.7 shows concentration at the outlet at different times before reaching a steady state at approximately 900 seconds.

Simulation contours for concentrations are shown in **Appendix A.1

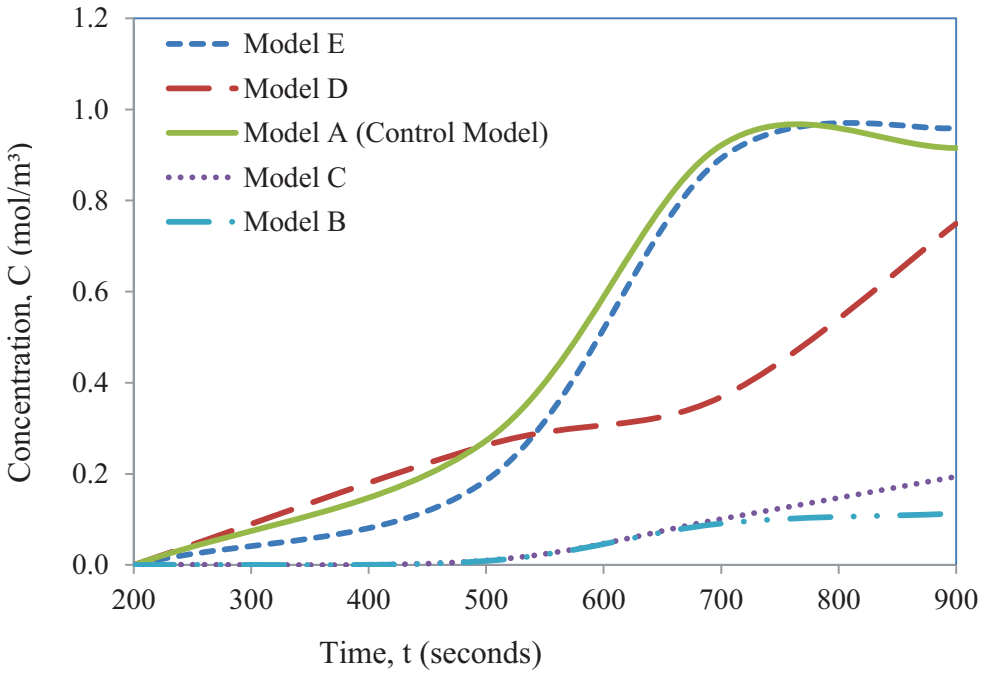

Figure 3.7 Concentration (mol/m³) distributions at different times at 200, 500, 700 and 900 seconds for control model A and models B through E

3.4 Summary

As mentioned earlier, this chapter reports geometrical modifications in the analysis chamber of the T-shaped microchannel and its effect on the fluid velocity. In addition, electrical and transient parametric analysis to maximize the species concentration was explored. Higher electric potentials and optimal microchannel size may be used to manipulate velocity and concentration distributions at the outlet due to electroosmosis process. Ionic fluid velocity and ion concentration showed promising results in order to design an effective microfluidic chip that may be used for mixing, pumping and detection purposes in bioanalytical applications.

CHAPTER 4

ANALYSIS OF ELECTROPHORETIC FLOW IN MICROFLUIDIC CHIPS *

Lab-on-chip devices are proven to be useful for many novel applications for the transport of the liquid samples and other supporting electrolyte solutions through the electrokinetically driven flow. One of the efficient methods for transporting liquid is through induced electrokinetic effects in response to an electric field across the inlets and outlet ports. Here mobilized ions are carried over in the microchannel with the application of electric fields through the entire solution from inlet via probe region for its detection and/or separation to outlet and the determination of concentration distribution at any analysis point in the channel. COMSOL, commercially available multiphysics software, with its specific MEMS and Chemical Engineering modules, was employed and simulated for the analysis of aqueous solution velocity and ionic concentration throughout the channel of various shapes.

As in the previous chapter, the ionic fluid concentrations and velocities in the channel and at the outlet are plotted against the potential differences across the two inlets in which analyte sample was introduced from one inlet and a buffer solution was supplied from another inlet. In addition, concentration distributions of the analytes were plotted against the various modes of analytes transport including diffusion, convection, electrophoretic migration plots were also made to investigate the electrophoretically driven flow of the analytes including concentration of analytes vs. zeta potential and the applied potential difference.

Keywords: Electrophoresis, Ionic Concentration and Multiphysics Software

*Partial Contents of this chapter was presented at 2012 American Society of Mechanical Engineers Summer Bioengineering (ASME-SBC) conference, June 20-23, 2012, Fajardo, Puerto Rico

4.1 Introduction

Micro Total Analysis (μTAS) systems have reserved a significant impact on the fields of bio-chemical analysis including detection, proteomics and clinical analysis (Oddy, 2005).To satisfy the demand for the accurate diagnosis of some specific genetic diseases, a method capable of providing high-accuracy, simplicity and high-quantity, rather than high-throughput would be desirable (Yamaguchi *et al.,* 2006). The micro total analysis system (μTAS) represents a suitable solution to address the above problem. Traditional methods to customize concentration distribution samples include filtration, centrifugation and extraction (Fong Lei *et al.,* 2009). Some of the concentration techniques in microfluidic system such as acoustic radiation pressure (Anderson *et al.,* 2002), micro sieving filters (Rijn *et al.,* 1999) and evaporation based concentrator (Walker & Beebe, 2002) has been published. However, because of the complicated fabrication processes for such techniques, it is cumbersome to integrate these concentration techniques into other laboratory processes such as sample preparation, amplification and detection of analytes. Meanwhile, it has been proven that electrokinetic forces such as AC electrothermal flow, electroosmosis, electrowetting, dielectrophoresis and electrophoresis can effectively manipulate bio-chemical analytes in aqueous solutions (Lian *et al.,* 2007, Bakewell & Morgan, 2006, Kang *et al.,* 2008, Cho *et al.,* 2003 and Ramos *et al.,* 1998).

Electrophoresis is an electrokinetic flow that describes the movement of charged particles suspended in fluid under an applied electric field (Fong Lei *et al.,* 2009). Different types of electrokinetic forces can be applied to drive fluid flow and manipulate bio-molecules chemical ions for analysis of many biological/chemical applications (Wong *et al.,* 2004). Majority of research groups both computational and laboratory based, have reported on

how to drive aqueous solution and analyze the concentration profiles of the analytes. Poisson-Nernst-Planck equations have been commonly used for the ionic mass transport and the Navier-Stokes equations are for the hydrodynamic flow field (Zhang *et al.,* 2010). In addition continuity equations for the fluid flow of aqueous solutions and for the ionic flux density of analytes govern the sample analytes with fluid media. The electrokinetic concentration profiles of the sample analytes and their controlled transport were previously reported (Daghight *et al.,* 2010). In the current chapter, computational modeling and simulations is mainly focused on the electrophoretic transport mode responsible for the concentration profiles of the sample analytes in the aqueous solution. Furthermore, results of other modes of ionic mass transport including convection, diffusion, and migration and in combination with electrophoretically driven transport are presented and compared.

4.2 Mathematical modeling

Based on the control model used from COMSOL library shown in Figure 4.1, micro machined surfaces of the channels of a biochip are formed with charged ions of the analytes. The counter ions are depleted next to the wall surfaces creating a thin layer called Debye layer. This layer is also referred to as a diffuse layer. The layer is dependent on the material used and formed by either negatively of positively charged groups the surfaces. The flow is expected to be laminar with of very low Reynolds number ($Re<10$). The derivations of governing fluid flow with boundary conditions are expressed in equations (4.1-4.6).

The slip boundary conditions are applied at the wall and electrical potentials are applied at two inlets across the outlet. An electrolyte solution of 3.07 mole/m^3 is fed with zero-concentrated species from other inlet. All physical constants are illustrated in Table 4.1:

Table 4.1 Physical constants used in COMSOL Multiphysics software

Symbols	Values	Descriptions
rho	1000[kg/m^3]	Density of water @STP
eta	1e-3[Pa*s]	Viscosity of water @STP
D	1e-9[m^2/s]	Ion diffusivity of Saline
Rg	8.314[J/(mol*K)]	Universal Gas constant
T	298[K]	Temperature of Sample solutions
nu	D/(Rg*T)	Ion mobility of Sample
sigma	1[S/m]	Electric conductivity electrolyte
c_in	0.05*3.5[g/l]/(22+35)[g/mol]	Inlet concentration of Sample
zeta0	0.3[V]	Initial Zeta Potential

Governing Equations

- **Physics of fluid flow**

a) Continuity:

$$\nabla \bullet u = 0 \qquad \text{..……(4.1)}$$

b) Navier-Stokes equations:

$$\rho\left[\frac{\partial u}{\partial t} + (u.\nabla)u\right] = -\nabla p + \mu\nabla^2 u + \rho_e \mathbf{E} \qquad \text{……(4.2)}$$

$$u_{Slip} = \frac{\varepsilon_0 \varepsilon_r \varsigma_0}{\eta}\mathbf{E} \qquad \text{……..(4.3)}$$

- **Physics of chemical mass transport**

c) Chemical mass-transport equations:

$$\frac{\partial c}{\partial t} + \nabla.(-D_i \nabla c_i - z_i u_{mi} F c_i \nabla V) = 0 \qquad \text{…….....……..(4.4)}$$

$$N_i = uc_i - D_i \nabla c_i - z_i m_i F c_i \nabla V \qquad \text{…….(4.5)}$$

$$\sum_{i=1}^{i} z_i c_i = 0 \qquad \text{……..(4.6)}$$

Where,

η denotes the dynamic viscosity (Pa·s),

u is the velocity (mm/s), N_k is the flux density,

E is the electric field intensity,

ρ denotes the fluid's density (kg/m^3),

p is the pressure (Pa),

ε_0 denotes the permittivity of free space (F/m),

ε_r is the relative permittivity of water (dimensionless),

ζ_0 refers to the zeta potential at the channel wall (V),

and V denotes the potential (V),

c_i is the concentration (mol/m^3),

D_i represents the diffusivity (m^2/s),

z_i equals the charge number (which equals 1 for this model),

u_{mi} is the mobility (s·mol/kg),

and F is Faraday's constant (C/mol).

Fig 4.1 depicts the model of microfluidic chip with modified geometry at the analysis chamber.

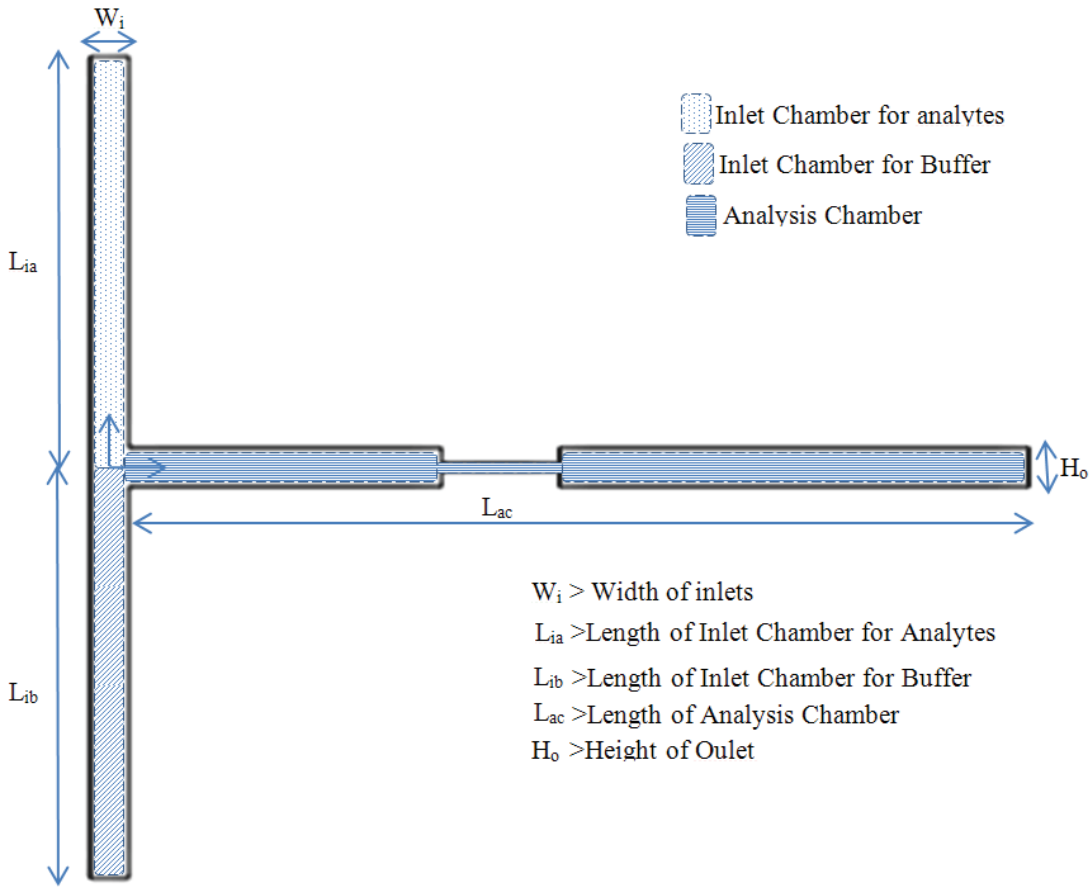

Figure 4.1 Microfluidic chip model D showing two injection and one analysis chambers

As shown in the figure, two injection chambers supply analytes and electrolytes and sample analyte solution is driven toward the outlet via analysis chamber sometimes called probe region. Considering drag on the moving analytes due to viscosity of the aqueous solution with low Reynolds number and moderate electric field strength E, the velocity of

the analytes v is simply proportional to the applied electric field. Thus induced mobility for the analytes, called as electrophoretic mobility, μ_{eo} defined as $\mu_{eo} = \frac{v}{E}$

According to Helmholtz-Smoluchowski's (1903) theory of electrophoresis $\mu_{eo} = -\frac{\varepsilon_r \varepsilon_o \varsigma}{\eta}$

and $v_{eo} = -\frac{\varepsilon_w \varepsilon_o \varsigma}{\eta} E$

where, ε_r: dielectric constant of medium (water), ε_o: Permittivity of free space, η: dynamic viscosity of water.

This is only valid for thin double layer and does not include the Debye length K^{-1}. However, Debye length is only a few nanometers for a aqueous solutions medium and the Smoluchouski's theory is still valid. The theory neglects surface conducting on the walls expressed by Dunkin number. Du<<1.

4.3 Results and discussion

First T-shaped DNA chip model of 0.25 mm also named as Control model, here with supporting electrolytes i.e. saline solution was modeled and simulated with known boundary conditions according to the published work (Jacobson *et al,*2002). The model was further analyzed with various electric potentials and zeta potentials as well. The two inlets were first applied electrical potentials of -3.5 V and -3.2 V with 0V at outlet in order to measure concentration distribution throughout the micro-channel.

4.3.1 Concentration profiles due to chemical mass transport modes (diffusion, convection, and electrophoretic migration flows)

The constant concentrations throughout the length of channel were achieved in diffusion and electrophoresis process. However concentration pattern seemed to be decreasing with length of the chip when convection mode was added in above processes. The concentration at the outlet due to convection and electrophoresis was obtained higher than that of diffusion and convection. Due to effect of migration of ions, electrophoresis process contributes maximum concentration all over the chip (Figure 4.2)

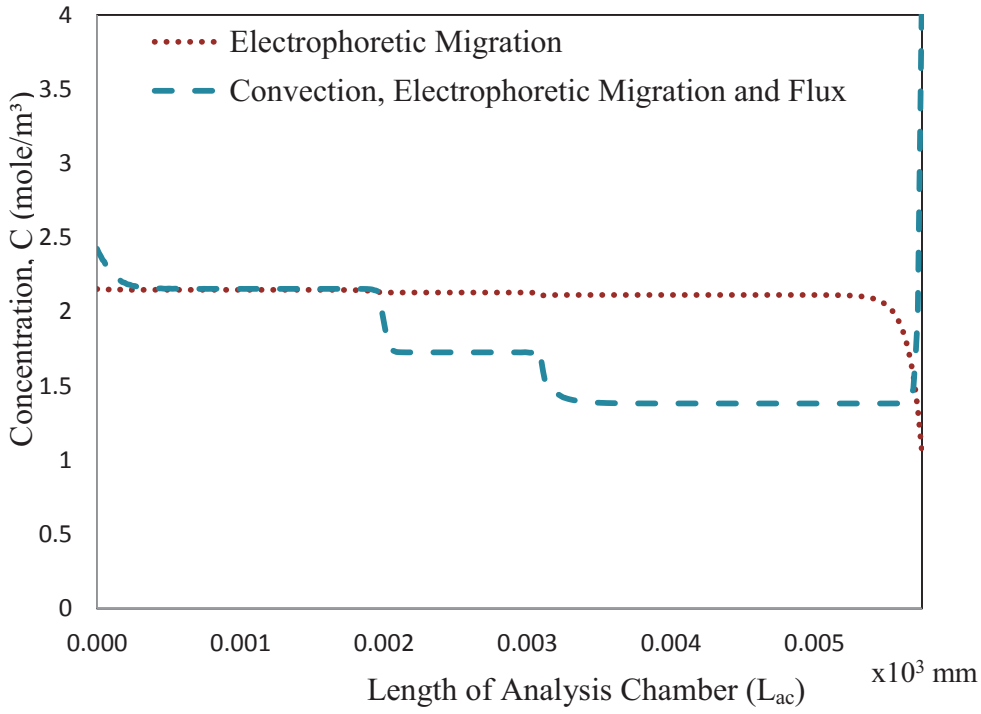

Figure 4.2 Concentration Vs length of analysis chamber of the chip for zeta potential= 0.3V ***

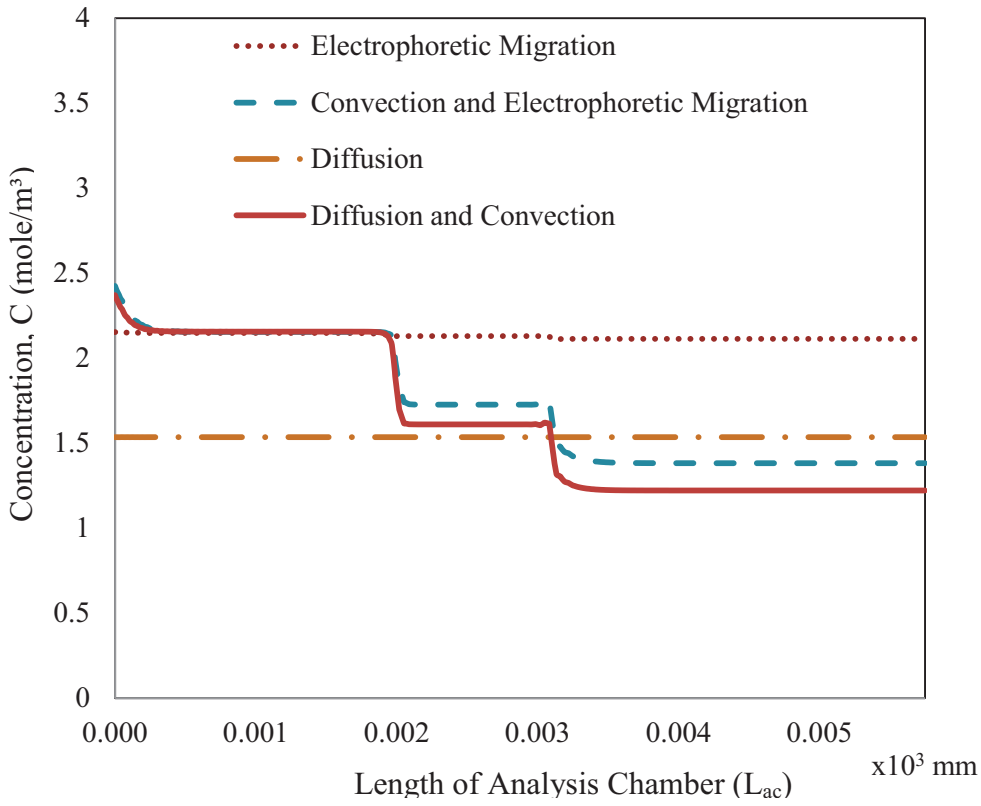

Figure 4.3 Concentration Vs length of analysis chamber of the chip for zeta potential= 0.3V ***

4.3.2 Effect of electrophoretic mobility on concentration distribution

When total flux of the analyte species was considered with two modes of mass transport namely convective and electrophoretic migration in combine, plot of average concentration at the outlet was seen highest. Thus combined effect of all the modes of transport compared to an individual mode of transport for the concentration distribution of analytes. Counteracting with electrophoretic transport of combined with one or two more transport modes, analyte concentrations will be less intense as seen in Figure 4.3.

***Simulation data sheets for chemical mass transport are shown in **Appendix A.2**

4.3.3 Effect of zeta potential on concentration distribution at the outlet

As shown in figure 4.4, increasing zeta potential also increases the electrophoretic mobility in the bulk solution of analytes resulting the higher peak.

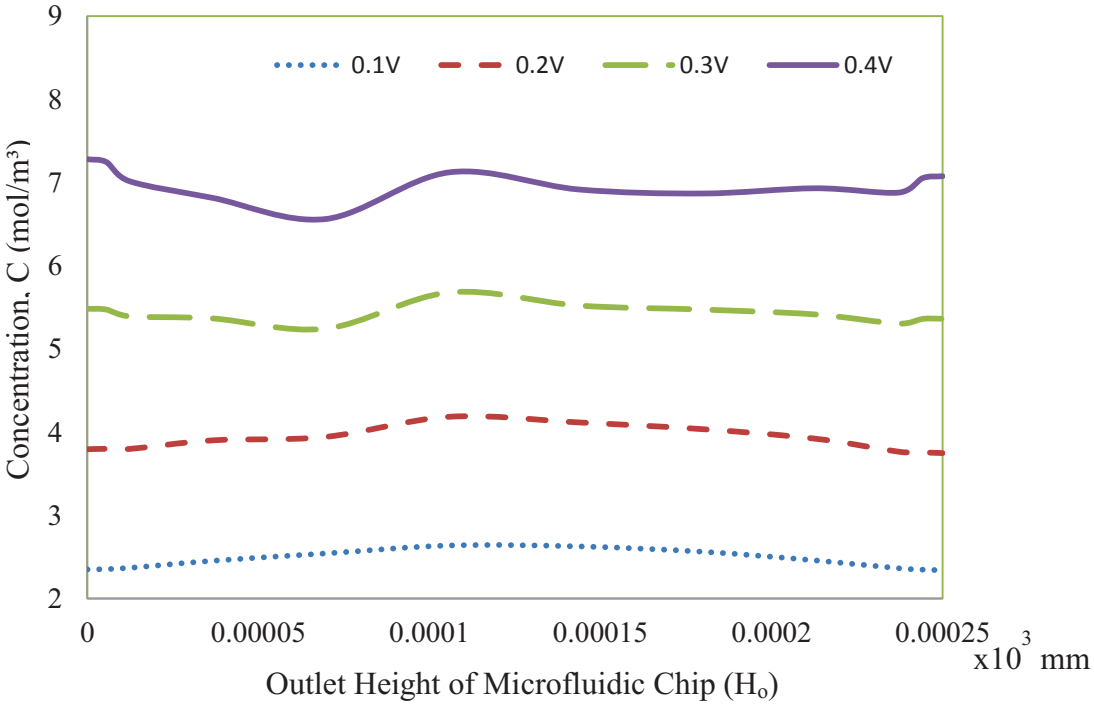

Figure 4.4 Concentration Vs height of a modified microfluidic chip applied with potential difference of -3.5V for inlet 1 and -3.2V for inlet2 at different zeta potentials (0.1V to 0.4 V)***

***Simulation data sheets for chemical mass transport are shown in **Appendix A.2**

4.3.4 Effect of potential difference on concentration distribution

Initial, DC voltage of -3.5V and -3.2 V were imposed at the upper and lower inlets respectively. Various Potential differences between two inlets were then applied to achieve maximum concentration at the outlet. The plot shown in Figure 4.5 depicts concentration at outlet of the microchannel.

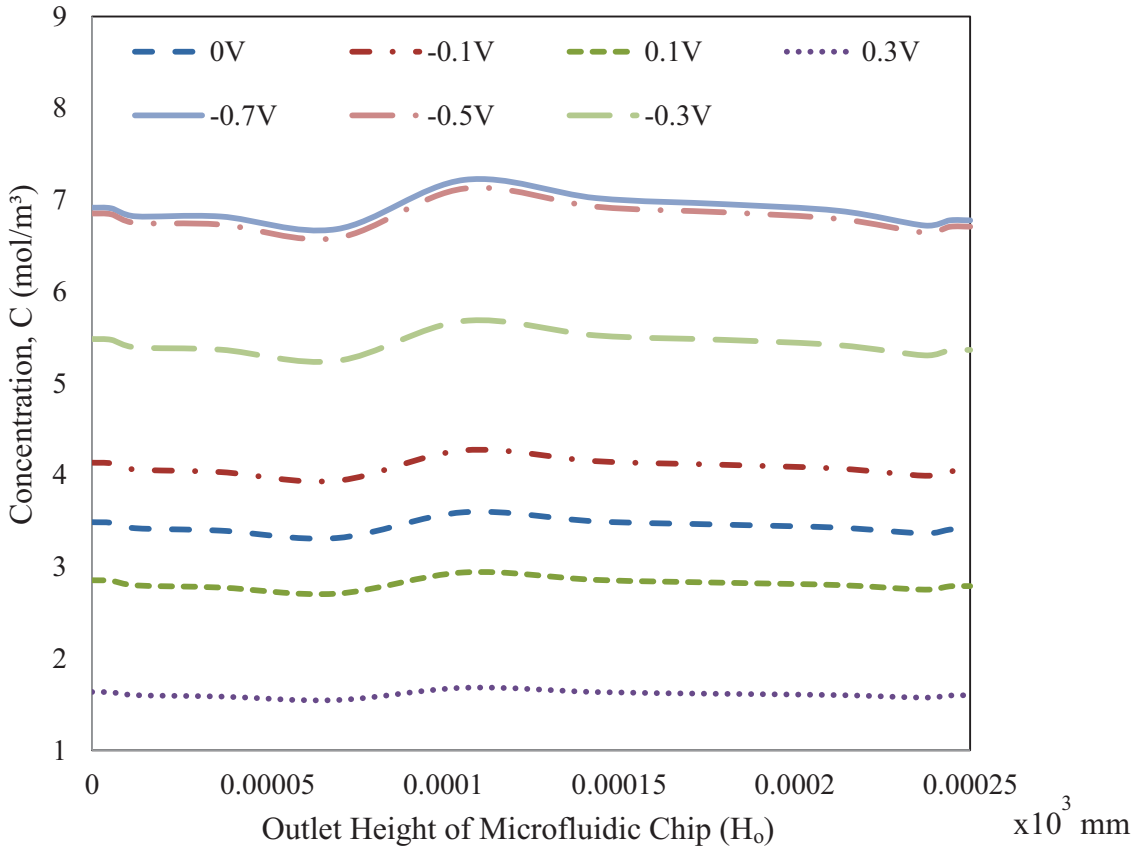

Figure 4.5 Concentration Vs outlet height of a modified microfluidic chip at various potential differences for two inlets at constant zeta potential of 0.3V***

***Simulation data sheets for chemical mass transport are shown in **Appendix A.2**

4.4 Summary

This chapter is focused on parametric analysis to maximize the analyte species concentration in a modified T-shaped DNA chips with reduced cross sectional area at the analysis chamber. Higher zeta potentials and species flux could be used to manipulate concentration distribution at the outlet due to electrophoresis process. Results of ionic concentration profiles demonstrate potential application to design a customized microsystem of optimal size with optimal modeling parameters that may be useful for the determination of concentration of analytes in a detectable range.

CHAPTER 5

CONCLUSIONS AND FUTURE WORKS

Common laboratory processes including injection, mixing, pumping, separating and detecting of sample analytes can be performed in a microfluidic chip known as Lab on Chip LOC (lab on a chip). LOC technology is becoming one of the concerns for Electrokinetic flow. LOCs are widely used in varieties of STEM disciplines that includes mechanical, chemical, bioengineering and sensor development areas. Majority of LOC devices are efficient, inexpensive, ease of operation, repeatable and reliable. However, there are some complexities associated with the flow mechanics including electroosmotic flow tend to be related to the relatively high potentials to generate significant low velocities.

With the better understanding of fluid flow physics and ionic mass transport phenomenon, by modeling and multiphysics simulation electrokinetic flow modes of ionic mass transport hold a great promise for LOC applications. Electrokinetic flow includes the transport of liquids (electroosmosis) and sample analytes (electrophoresis) in response to an applied electric field. Both modes of motions are closely associated with the electric double layer (EDL) that is automatically generated at the solid-liquid interference in which there is a net charge density. Electrokinetic flow that has the capability of combined electroosmosis and electrophoresis transport modes, is more suited to miniaturized LOC applications in comparison to a traditional pressure-driven flow. Electrokinetic flow produces a nearly plug like velocity profile and much lower flow resistance which can eventually be useful for producing higher ion detection signals

when applying higher electric potentials. However, Joule heating and bubble generation are ubiquitous phenomenon in electrokinetic flow which can affect the aqueous solution and sample analytes transport via temperature sensitive materials.Recalling conclusions and summary of results from each chapter, following are some important findings:

- When the applied potential is high, the maximum ionic fluid velocity increases keeping a constant zeta potential. The modified micro-chip (Model B) has maximum ionic fluid velocity that increases in zeta potentials.
- Concentration distribution could be manipulated at the outlet with convective electrophoretic migration modes with net species flux. If the net species ionic flux (due to diffusion, convection and migration)is more than the flux out from the exit then there may be accumulation of species concentration. This is local statement and was not thoroughly verified and, or validated in this work.
- Maximum species accumulation i.e. high concentration of species may be achieved by increasing zeta potential values.
- A minimal effect of microfluidic chip on concentration distribution was seen. However, the average maximum velocity is influenced be shape and size of the chip at different locations of the microchannel. This was true especially at the analysis chamber of each microchip models A through E.

This topic of research is wide open and still needs more investigation that points a number of future research. A thorough parametric analysis and a comparative study with other modes of mass transport can be done. In addition, optimization of the electroosmosis and electrophoresis should be performed to utilize the electrokinetic modes of transport for a number of bioanalytical applications.

REFERENCES

Y.M. Panta, S. Qian, J. Liu, M.A.Cheney, S.W. Joo, “Ultrasensitive detection of mercury(II) ions using electrochemical surface plasmon resonance with magnetohydrodynamic convection”, J Colloid Interface Sci. 333(2009), 485-90.

Y.M. Panta, D.E. Farmer, P. Johnson, M.A.Cheney, S. Qian, “Preparation of alpha sources using magnetohydrodynamic electrodeposition for radionuclide metrology”, J Colloid Interface Sci. 342(2010), 128-134.

Y.M. Panta, S. Qian, M.A.Cheney, “Stripping analysis of mercury(II) ionic solutions under magneto-hydrodynamic convection”, J Colloid Interface Sci. 317(2008), 175-182.

M.H. Oddy, "Electrokinetic Transport Phenomena: Mobilty Measurement and Electrokinetic Instability". Ph. D dissertation, Stanford University, 2005.

Y. Yamaguchi, D. Ogura , K. Yamashita , M. Miyazaki, H. Nakamuraa, H. Maeda, "A method for DNA detection in a microchannel: Fluid dynamics phenomena and optimization of microchannel structure", Talanta 68 (2006), 700–707

K.F. Lei , H. Cheng,, K.Y. Choy, Larry M.C. Chow, "Electrokinetic DNA concentration in microsystems", Sensors and Actuators A 156 (2009), 381–387.

M.J. Anderson, R.S. Budwig, K.S. Line, J.G. Frankel, "Use of acoustic radiation pressure to concentrate small particles in an air flow", IEEE Ultrasonics Symp. (2002) 481–484.

C.J.M. Van Rijn, W. Nijdam, S. Kuiper, G.J. Veldhuis, H. ven Wolferen, M. Elwenspoek, "Microsieves made with laser interference lithography for microfiltration application", J. Micromech. Microeng. 9 (1999),170–172

G.M. Walker, D.J. Beebe, "An evaporation-based microfluidic sample concentration method", Lab Chip 2 (2002), 57–61.

M. Lian, N. Islam, J. Wu, "AC electrothermal manipulation of conductive fluids and particles for lab-chip applications", IET Nanobiotechnol. 1 (3) (2007), 36–43.

D.J. Bakewell, H. Morgan, "Dielectrophoresis of DNA: time-and frequencydependent collections on microelectrodes", IEEE Trans. Nanobiosci. 5 (1) (2006), 1–8

Y. Kang, D. Li, S.A. Kalams, J.E. Eid, "DC-dielectrophoretic separation of biological cells by size", Biomed. Microdevices 10 (2008), 243–249.

S.K. Cho, H. Moon, C.J. Kim, "Creating, transporting, cutting and merging liquid droplets by electrowetting-based actuation for digital microfluidic circuits", IEEE J. Microelectromech. Syst. 12 (2003), 70–80

A. Ramos, H. Morgan, N.G. Green, A. Castellanos, "AC electrokinetics: a review of forces in microelectrode structures", J. Phys. D: Appl. Phys. 31 (1998) ,2338–2353.

P.K. Wong, T.H. Wang, J.H. Deval, C.M. Ho, "Electrokinetics in microdevices for biotechnology applications", Trans. Mechatron. 9 (2004), 366–376.

Y. Ai, Liu, J., Zhang, B.K., and Qian, S., “Field Effect Regulation of DNA Translocation through a Nanopore” Journal of Analytical Chemistry, 82(2010), 8217-8225

Y. Daghighi, D. Li, “Numerical Studies of ELectrokinetic Control of DNA Concentration in a Closed-end Microchannel" *Electrophoresis* 2010, 31, 868–878.

J.M. MacInnes, “Computation of reacting electrokinetic flow in microchannel geometries’’ Journal of Chemical Engineering Science, 57 (2002), 4539-4558.

M. Georgiadou, “Modeling current density distribution in electrochemical systems,” Electrochim. Acta 48 (2003), 4089.

H. Kabbani, A. Wang, X. Luo, S. Qian, “Modeling RedOx-based magnetohydrodynamics in three-dimensional microfluidic channels”,Phys. Fluids 19 (2007), 083604

D.J. Harrison, K. Fluri, K. Seiler, Z. Fan, C.S. Effenhauser, A. Manz, Science, 261 (1993), 895

S.K.W. Dertinger, D.T. Chiu, N.L. Jeon, G.M. Whitesides, Anal. Chem., 73 (2001), 1240.

Addressing *http://www.comsol.com*, retrieved on 01/15/11

APPENDIX

A.1 SIMULATION CONTOURS FOR VELOCITY AND CONCENTRATION

CONCENTRATION CONTOURS FOR DIFFERENT MODES OF MASS TRANSPORT

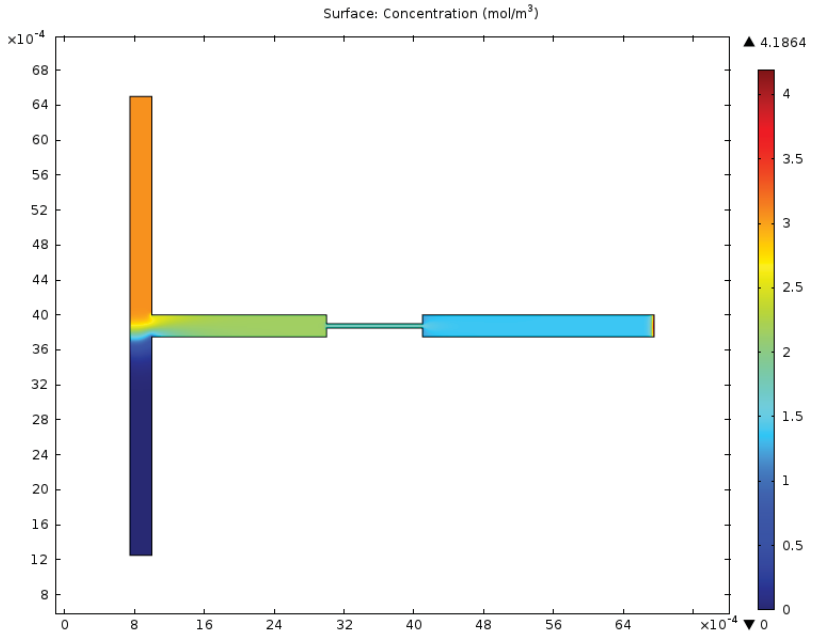

Figure A.1.1 Convection with electrophoretic migration with species flux mode

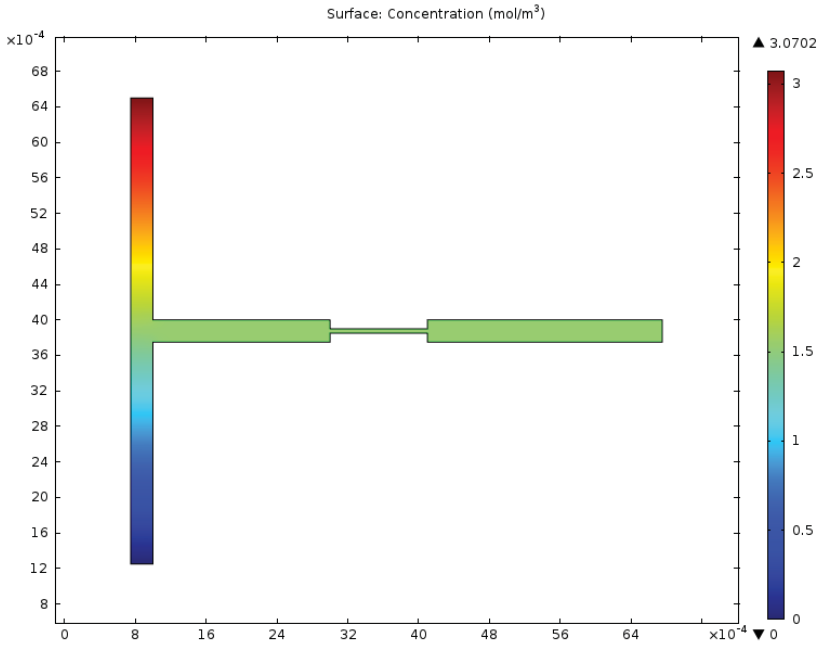

Figure A.1.2 Diffusion mode

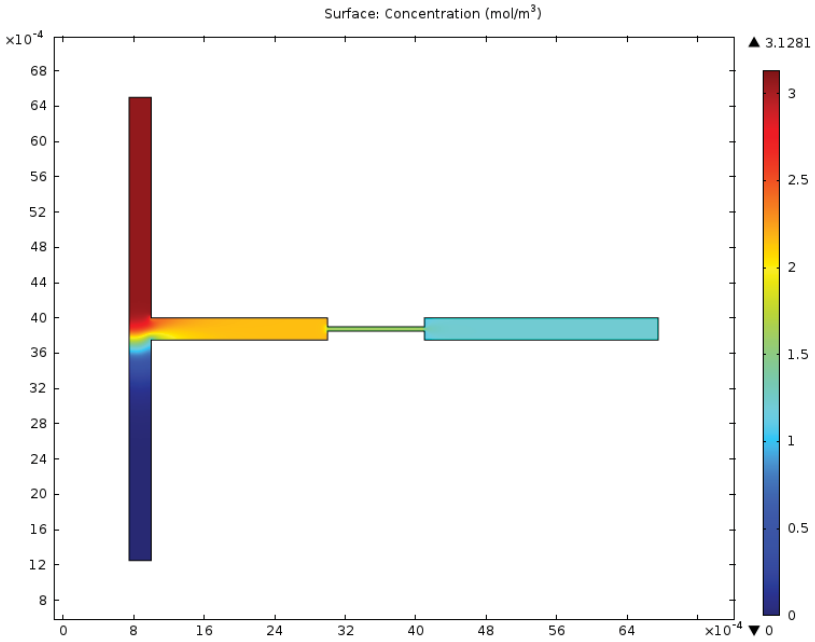

Figure A.1.3 Diffusion and convection mode

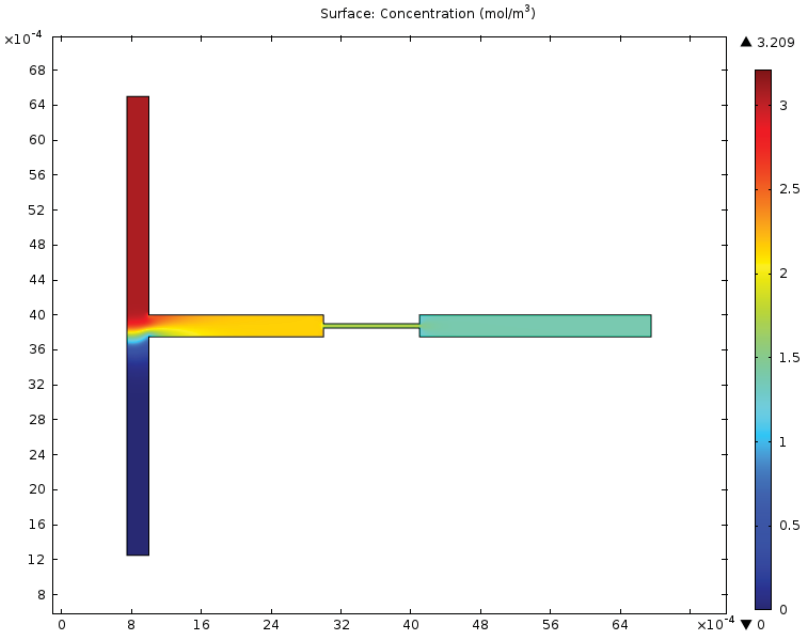

Figure A.1.4 Convection and electrophoretic migration mode

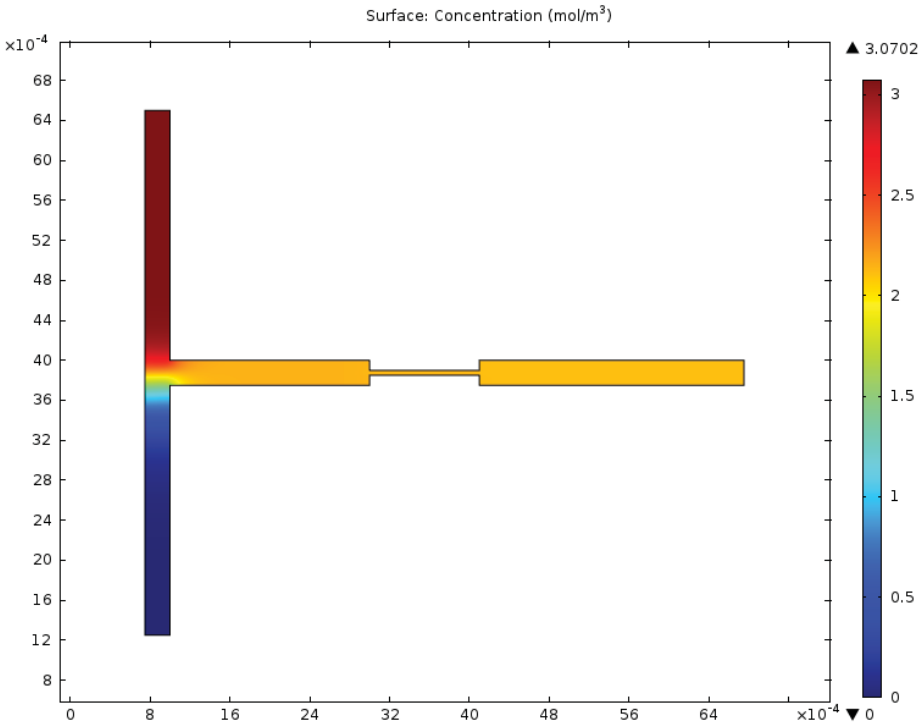

Figure A.1.5 Electrophoretic migration in electric field mode

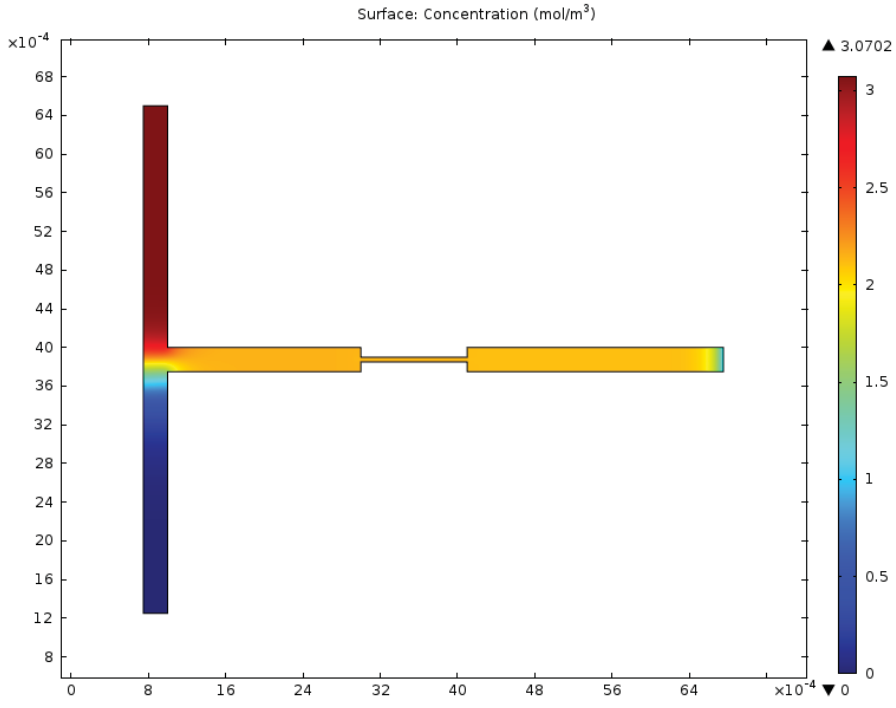

Figure A.1.6 Electrophoretic migration with species flux in electric field mode

VELOCITY CONTOURS

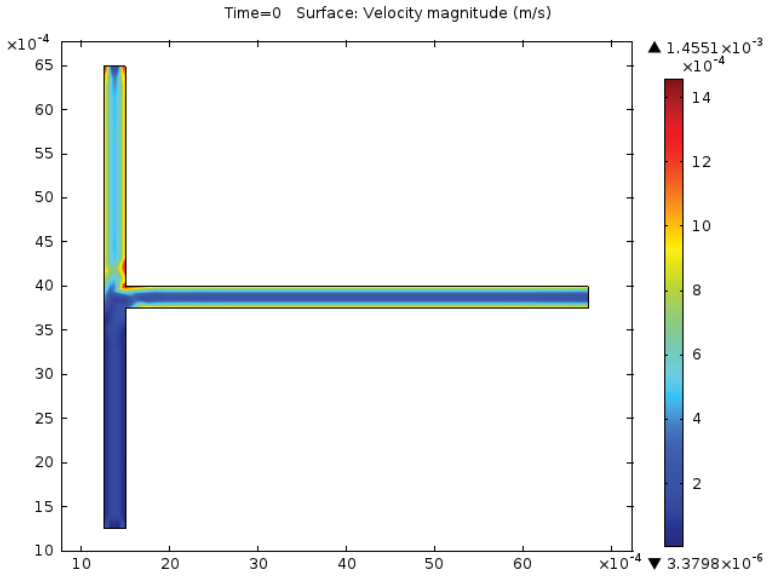

Figure A.1.7 Velocity contours at initial condition

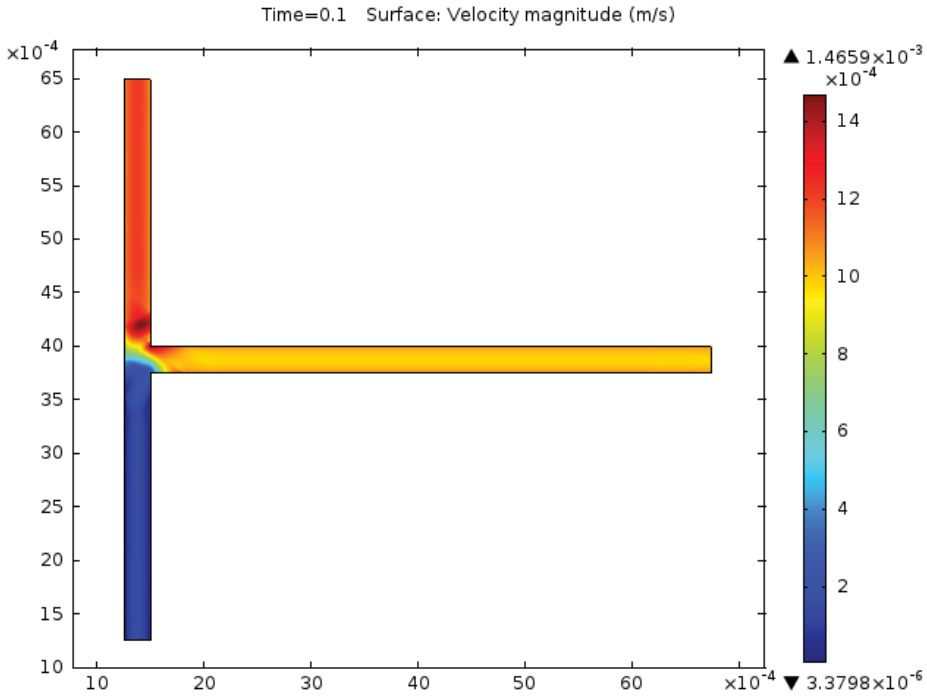

Figure A.1.8 Velocity contours at time=0.1 second

A.2 SIMULATION DATA SHEETS FOR CHEMICAL MASS TRANSPORT

Table A.2.1 Concentration at different point of analysis chamber for model D

Length of Chip (m)	Electrophoresitic Migration and Flux (mol/m³)	Electrophoresis Migration (mol/m³)	Convection, Diffusion, Electrophoretic Migration and Flux (mol/m³)	Convection and Electrophoretic Migration (mol/m³)	Diffusion (mol/m³)	Diffusion and Convection (mol/m³)
0	2.153	2.153	2.425	2.425	1.535	2.371
0.00001	2.152	2.152	2.400	2.400	1.535	2.347
0.00003	2.149	2.149	2.372	2.372	1.535	2.319
0.00004	2.151	2.151	2.349	2.349	1.535	2.298
0.00005	2.153	2.153	2.337	2.337	1.535	2.287
0.00007	2.148	2.148	2.297	2.297	1.535	2.253
0.00009	2.152	2.152	2.279	2.279	1.535	2.238
0.00011	2.147	2.147	2.254	2.254	1.535	2.218
0.00012	2.151	2.151	2.241	2.241	1.535	2.208
0.00014	2.147	2.147	2.223	2.223	1.535	2.195
0.00016	2.150	2.150	2.214	2.214	1.535	2.189
0.00018	2.147	2.147	2.200	2.200	1.535	2.180
0.00019	2.149	2.149	2.195	2.195	1.535	2.177
0.00021	2.147	2.147	2.185	2.185	1.535	2.170
0.00023	2.149	2.149	2.183	2.183	1.535	2.169
0.00025	2.147	2.147	2.175	2.175	1.535	2.165
0.00026	2.149	2.149	2.174	2.174	1.535	2.165
0.00028	2.147	2.147	2.168	2.168	1.535	2.161
0.00030	2.148	2.148	2.168	2.168	1.535	2.162
0.00032	2.148	2.148	2.163	2.163	1.535	2.159
0.00033	2.148	2.148	2.164	2.164	1.535	2.160
0.00035	2.148	2.148	2.160	2.160	1.535	2.158
0.00037	2.148	2.148	2.161	2.161	1.535	2.158
0.00039	2.148	2.148	2.158	2.158	1.535	2.157

Length of Chip (m)	Electrophoresitic Migration and Flux (mol/m^3)	Electrophoresis Migration (mol/m^3)	Convection, Diffusion, Electrophoretic Migration and Flux (mol/m^3)	Convection and Electrophoretic Migration (mol/m^3)	Diffusion (mol/m^3)	Diffusion and Convection (mol/m^3)
0.00041	2.148	2.148	2.159	2.159	1.535	2.158
0.00042	2.148	2.148	2.157	2.157	1.535	2.156
0.00045	2.148	2.148	2.158	2.158	1.535	2.157
0.00046	2.148	2.148	2.156	2.156	1.535	2.156
0.00047	2.148	2.148	2.155	2.155	1.535	2.156
0.00049	2.148	2.148	2.156	2.156	1.535	2.156
0.00050	2.148	2.148	2.157	2.157	1.535	2.157
0.00053	2.148	2.148	2.155	2.155	1.535	2.156
0.00054	2.148	2.148	2.156	2.156	1.535	2.156
0.00056	2.148	2.148	2.155	2.155	1.535	2.156
0.00059	2.148	2.148	2.155	2.155	1.535	2.156
0.00060	2.148	2.148	2.155	2.155	1.535	2.156
0.00061	2.148	2.148	2.154	2.154	1.535	2.156
0.00063	2.148	2.148	2.155	2.155	1.535	2.156
0.00065	2.148	2.148	2.154	2.154	1.535	2.156
0.00067	2.148	2.148	2.155	2.155	1.535	2.156
0.00069	2.148	2.148	2.155	2.155	1.535	2.156
0.00070	2.148	2.148	2.154	2.154	1.535	2.156
0.00072	2.148	2.148	2.154	2.154	1.535	2.156
0.00074	2.148	2.148	2.155	2.155	1.535	2.156
0.00075	2.148	2.148	2.155	2.155	1.535	2.156
0.00077	2.148	2.148	2.154	2.154	1.535	2.156
0.00079	2.148	2.148	2.155	2.155	1.535	2.156
0.00081	2.148	2.148	2.154	2.154	1.535	2.156

Length of Chip (m)	Electrophoresitic Migration and Flux (mol/m^3)	Electrophoresis Migration (mol/m^3)	Convection, Diffusion, Electrophoretic Migration and Flux (mol/m^3)	Convection and Electrophoretic Migration (mol/m^3)	Diffusion (mol/m^3)	Diffusion and Convection (mol/m^3)
0.00084	2.148	2.148	2.154	2.154	1.535	2.156
0.00085	2.148	2.148	2.154	2.154	1.535	2.156
0.00088	2.148	2.148	2.155	2.155	1.535	2.156
0.00090	2.148	2.148	2.154	2.154	1.535	2.156
0.00091	2.148	2.148	2.154	2.154	1.535	2.156
0.00092	2.148	2.148	2.155	2.155	1.535	2.156
0.00095	2.148	2.148	2.154	2.154	1.535	2.156
0.00097	2.148	2.148	2.155	2.155	1.535	2.156
0.00098	2.148	2.148	2.154	2.154	1.535	2.156
0.00101	2.148	2.148	2.155	2.155	1.535	2.156
0.00102	2.148	2.148	2.154	2.154	1.535	2.156
0.00103	2.148	2.148	2.154	2.154	1.535	2.156
0.00105	2.148	2.148	2.154	2.154	1.535	2.156
0.00108	2.148	2.148	2.154	2.154	1.535	2.156
0.00109	2.148	2.148	2.154	2.154	1.535	2.156
0.00110	2.148	2.148	2.155	2.155	1.535	2.156
0.00112	2.148	2.148	2.154	2.154	1.535	2.156
0.00115	2.148	2.148	2.154	2.154	1.535	2.156
0.00116	2.148	2.148	2.154	2.154	1.535	2.156
0.00118	2.148	2.148	2.154	2.154	1.535	2.156
0.00119	2.148	2.148	2.154	2.154	1.535	2.156
0.00120	2.148	2.148	2.154	2.154	1.535	2.156
0.00123	2.148	2.148	2.154	2.154	1.535	2.156
0.00125	2.148	2.148	2.154	2.154	1.535	2.156

Length of Chip (m)	Electrophoresitic Migration and Flux (mol/m^3)	Electrophoresis Migration (mol/m^3)	Convection, Diffusion, Electrophoretic Migration and Flux (mol/m^3)	Convection and Electrophoretic Migration (mol/m^3)	Diffusion (mol/m^3)	Diffusion and Convection (mol/m^3)
0.00126	2.148	2.148	2.154	2.154	1.535	2.156
0.00129	2.148	2.148	2.154	2.154	1.535	2.156
0.00130	2.148	2.148	2.154	2.154	1.535	2.156
0.00131	2.148	2.148	2.154	2.154	1.535	2.156
0.00133	2.148	2.148	2.154	2.154	1.535	2.156
0.00135	2.148	2.148	2.154	2.154	1.535	2.156
0.00137	2.148	2.148	2.154	2.154	1.535	2.156
0.00139	2.148	2.148	2.154	2.154	1.535	2.156
0.00141	2.148	2.148	2.154	2.154	1.535	2.156
0.00142	2.148	2.148	2.154	2.154	1.535	2.156
0.00144	2.148	2.148	2.154	2.154	1.535	2.156
0.00146	2.148	2.148	2.154	2.154	1.535	2.156
0.00148	2.148	2.148	2.154	2.154	1.535	2.156
0.00149	2.148	2.148	2.154	2.154	1.535	2.156
0.00151	2.148	2.148	2.154	2.154	1.535	2.156
0.00153	2.148	2.148	2.154	2.154	1.535	2.156
0.00154	2.148	2.148	2.154	2.154	1.535	2.156
0.00155	2.148	2.148	2.154	2.154	1.535	2.156
0.00158	2.148	2.148	2.154	2.154	1.535	2.156
0.00160	2.148	2.148	2.154	2.154	1.535	2.156
0.00161	2.148	2.148	2.154	2.154	1.535	2.156
0.00164	2.148	2.148	2.154	2.154	1.535	2.156
0.00165	2.148	2.148	2.154	2.154	1.535	2.156
0.00166	2.147	2.147	2.154	2.154	1.535	2.156

Length of Chip (m)	Electrophoresitic Migration and Flux (mol/m³)	Electrophoresis Migration (mol/m³)	Convection, Diffusion, Electrophoretic Migration and Flux (mol/m³)	Convection and Electrophoretic Migration (mol/m³)	Diffusion (mol/m³)	Diffusion and Convection (mol/m³)
0.00168	2.147	2.147	2.154	2.154	1.535	2.156
0.00170	2.147	2.147	2.154	2.154	1.535	2.156
0.00172	2.147	2.147	2.154	2.154	1.535	2.156
0.00174	2.147	2.147	2.154	2.154	1.535	2.156
0.00175	2.147	2.147	2.154	2.154	1.535	2.156
0.00177	2.146	2.146	2.154	2.154	1.535	2.156
0.00179	2.146	2.146	2.154	2.154	1.535	2.156
0.00181	2.146	2.146	2.154	2.154	1.535	2.155
0.00182	2.145	2.145	2.154	2.154	1.535	2.155
0.00183	2.145	2.145	2.154	2.154	1.535	2.155
0.00185	2.144	2.144	2.154	2.154	1.535	2.154
0.00188	2.143	2.143	2.154	2.154	1.535	2.152
0.00188	2.142	2.142	2.154	2.154	1.535	2.152
0.00189	2.142	2.142	2.153	2.153	1.535	2.150
0.00192	2.139	2.139	2.151	2.151	1.535	2.143
0.00193	2.137	2.137	2.145	2.145	1.535	2.132
0.00194	2.136	2.136	2.144	2.144	1.535	2.127
0.00195	2.135	2.135	2.142	2.142	1.535	2.114
0.00197	2.133	2.133	2.129	2.129	1.535	2.078
0.00199	2.128	2.128	2.010	2.010	1.535	1.919
0.00199	2.128	2.128	1.988	1.987	1.535	1.892
0.00202	2.132	2.132	1.838	1.838	1.535	1.699
0.00202	2.132	2.132	1.833	1.833	1.535	1.694
0.00205	2.129	2.129	1.741	1.741	1.535	1.616

Length of Chip (m)	Electrophoresitic Migration and Flux (mol/m³)	Electrophoresis Migration (mol/m³)	Convection, Diffusion, Electrophoretic Migration and Flux (mol/m³)	Convection and Electrophoretic Migration (mol/m³)	Diffusion (mol/m³)	Diffusion and Convection (mol/m³)
0.00206	2.129	2.129	1.741	1.741	1.535	1.617
0.00209	2.130	2.130	1.729	1.729	1.535	1.611
0.00209	2.130	2.130	1.729	1.729	1.535	1.611
0.00212	2.130	2.130	1.727	1.727	1.535	1.610
0.00212	2.130	2.130	1.727	1.727	1.535	1.610
0.00216	2.130	2.130	1.726	1.726	1.535	1.610
0.00216	2.130	2.130	1.726	1.726	1.535	1.610
0.00219	2.130	2.130	1.726	1.726	1.535	1.610
0.00219	2.130	2.130	1.726	1.726	1.535	1.610
0.00222	2.130	2.130	1.726	1.726	1.535	1.610
0.00222	2.130	2.130	1.726	1.726	1.535	1.610
0.00226	2.130	2.130	1.726	1.726	1.535	1.610
0.00226	2.130	2.130	1.726	1.726	1.535	1.610
0.00229	2.130	2.130	1.726	1.726	1.535	1.610
0.00229	2.130	2.130	1.726	1.726	1.535	1.610
0.00232	2.130	2.130	1.726	1.726	1.535	1.610
0.00232	2.130	2.130	1.726	1.726	1.535	1.610
0.00236	2.130	2.130	1.726	1.726	1.535	1.610
0.00236	2.130	2.130	1.726	1.726	1.535	1.610
0.00239	2.130	2.130	1.726	1.726	1.535	1.610
0.00239	2.130	2.130	1.726	1.726	1.535	1.610
0.00243	2.130	2.130	1.726	1.726	1.535	1.610
0.00243	2.130	2.130	1.726	1.726	1.535	1.610
0.00246	2.130	2.130	1.726	1.726	1.535	1.610

Length of Chip (m)	Electrophoresitic Migration and Flux (mol/m^3)	Electrophoresis Migration (mol/m^3)	Convection, Diffusion, Electrophoretic Migration and Flux (mol/m^3)	Convection and Electrophoretic Migration (mol/m^3)	Diffusion (mol/m^3)	Diffusion and Convection (mol/m^3)
0.00246	2.130	2.130	1.726	1.726	1.535	1.610
0.00249	2.130	2.130	1.726	1.726	1.535	1.610
0.00249	2.130	2.130	1.726	1.726	1.535	1.610
0.00253	2.130	2.130	1.726	1.726	1.535	1.610
0.00253	2.130	2.130	1.726	1.726	1.535	1.610
0.00256	2.130	2.130	1.726	1.726	1.535	1.610
0.00256	2.130	2.130	1.726	1.726	1.535	1.610
0.00259	2.130	2.130	1.726	1.726	1.535	1.610
0.00259	2.130	2.130	1.726	1.726	1.535	1.610
0.00262	2.130	2.130	1.726	1.726	1.535	1.610
0.00262	2.130	2.130	1.726	1.726	1.535	1.610
0.00265	2.130	2.130	1.726	1.726	1.535	1.610
0.00266	2.130	2.130	1.726	1.726	1.535	1.610
0.00267	2.130	2.130	1.726	1.726	1.535	1.610
0.00267	2.130	2.130	1.726	1.726	1.535	1.610
0.00269	2.130	2.130	1.726	1.726	1.535	1.610
0.00271	2.130	2.130	1.726	1.726	1.535	1.610
0.00271	2.130	2.130	1.726	1.726	1.535	1.610
0.00272	2.130	2.130	1.726	1.726	1.535	1.610
0.00274	2.130	2.130	1.726	1.726	1.535	1.610
0.00275	2.130	2.130	1.726	1.726	1.535	1.610
0.00276	2.130	2.130	1.726	1.726	1.535	1.610
0.00277	2.130	2.130	1.726	1.726	1.535	1.610
0.00279	2.130	2.130	1.726	1.726	1.535	1.610

Length of Chip (m)	Electrophoresitic Migration and Flux (mol/m³)	Electrophoresis Migration (mol/m³)	Convection, Diffusion, Electrophoretic Migration and Flux (mol/m³)	Convection and Electrophoretic Migration (mol/m³)	Diffusion (mol/m³)	Diffusion and Convection (mol/m³)
0.00280	2.130	2.130	1.726	1.726	1.535	1.610
0.00281	2.130	2.130	1.726	1.726	1.535	1.610
0.00283	2.130	2.130	1.726	1.726	1.535	1.610
0.00284	2.130	2.130	1.726	1.726	1.535	1.610
0.00285	2.130	2.130	1.726	1.726	1.535	1.610
0.00286	2.130	2.130	1.726	1.726	1.535	1.610
0.00288	2.130	2.130	1.726	1.726	1.535	1.610
0.00288	2.130	2.130	1.726	1.726	1.535	1.610
0.00289	2.130	2.130	1.726	1.726	1.535	1.610
0.00292	2.130	2.130	1.726	1.726	1.535	1.610
0.00292	2.130	2.130	1.727	1.727	1.535	1.610
0.00295	2.130	2.130	1.726	1.726	1.535	1.610
0.00295	2.130	2.130	1.726	1.726	1.535	1.610
0.00299	2.130	2.130	1.728	1.728	1.535	1.612
0.00299	2.130	2.130	1.728	1.728	1.535	1.612
0.00301	2.130	2.130	1.725	1.725	1.535	1.608
0.00302	2.130	2.130	1.724	1.724	1.535	1.605
0.00302	2.130	2.130	1.724	1.724	1.535	1.605
0.00304	2.129	2.129	1.725	1.725	1.535	1.614
0.00305	2.128	2.128	1.726	1.726	1.535	1.621
0.00305	2.128	2.128	1.726	1.726	1.535	1.621
0.00308	2.127	2.127	1.752	1.751	1.535	1.615
0.00308	2.127	2.127	1.751	1.750	1.535	1.613
0.00311	2.110	2.110	1.593	1.592	1.535	1.440

Length of Chip (m)	Electrophoresitic Migration and Flux (mol/m³)	Electrophoresis Migration (mol/m³)	Convection, Diffusion, Electrophoretic Migration and Flux (mol/m³)	Convection and Electrophoretic Migration (mol/m³)	Diffusion (mol/m³)	Diffusion and Convection (mol/m³)
0.00311	2.110	2.110	1.592	1.591	1.535	1.439
0.00313	2.113	2.113	1.496	1.495	1.535	1.319
0.00316	2.112	2.112	1.482	1.482	1.535	1.306
0.00316	2.112	2.112	1.477	1.477	1.535	1.302
0.00316	2.112	2.112	1.476	1.476	1.535	1.301
0.00319	2.113	2.113	1.449	1.449	1.535	1.275
0.00322	2.113	2.113	1.441	1.441	1.535	1.266
0.00322	2.113	2.113	1.440	1.440	1.535	1.266
0.00322	2.113	2.113	1.440	1.440	1.535	1.266
0.00325	2.113	2.113	1.424	1.424	1.535	1.252
0.00326	2.113	2.113	1.420	1.420	1.535	1.249
0.00328	2.113	2.113	1.414	1.414	1.535	1.244
0.00329	2.113	2.113	1.410	1.410	1.535	1.241
0.00331	2.113	2.113	1.406	1.406	1.535	1.237
0.00333	2.113	2.113	1.403	1.403	1.535	1.235
0.00335	2.113	2.113	1.400	1.400	1.535	1.233
0.00337	2.113	2.113	1.397	1.397	1.535	1.231
0.00338	2.113	2.113	1.395	1.395	1.535	1.229
0.00340	2.113	2.113	1.394	1.394	1.535	1.229
0.00341	2.113	2.113	1.392	1.392	1.535	1.227
0.00343	2.113	2.113	1.391	1.391	1.535	1.227
0.00345	2.113	2.113	1.389	1.389	1.535	1.225
0.00347	2.113	2.113	1.388	1.388	1.535	1.225
0.00348	2.113	2.113	1.387	1.387	1.535	1.224

Length of Chip (m)	Electrophoresitic Migration and Flux (mol/m^3)	Electrophoresis Migration (mol/m^3)	Convection, Diffusion, Electrophoretic Migration and Flux (mol/m^3)	Convection and Electrophoretic Migration (mol/m^3)	Diffusion (mol/m^3)	Diffusion and Convection (mol/m^3)
0.00350	2.113	2.113	1.387	1.387	1.535	1.224
0.00352	2.113	2.113	1.386	1.386	1.535	1.223
0.00353	2.113	2.113	1.386	1.386	1.535	1.223
0.00355	2.113	2.113	1.385	1.385	1.535	1.223
0.00358	2.113	2.113	1.384	1.384	1.535	1.223
0.00359	2.113	2.113	1.384	1.384	1.535	1.222
0.00360	2.113	2.113	1.384	1.384	1.535	1.222
0.00362	2.113	2.113	1.384	1.384	1.535	1.222
0.00364	2.113	2.113	1.383	1.383	1.535	1.222
0.00366	2.113	2.113	1.383	1.383	1.535	1.222
0.00368	2.113	2.113	1.383	1.383	1.535	1.222
0.00369	2.113	2.113	1.383	1.383	1.535	1.222
0.00371	2.113	2.113	1.383	1.383	1.535	1.222
0.00373	2.113	2.113	1.383	1.383	1.535	1.222
0.00374	2.113	2.113	1.383	1.383	1.535	1.222
0.00376	2.113	2.113	1.382	1.382	1.535	1.222
0.00378	2.113	2.113	1.382	1.382	1.535	1.222
0.00380	2.113	2.113	1.382	1.382	1.535	1.222
0.00382	2.113	2.113	1.382	1.382	1.535	1.222
0.00383	2.113	2.113	1.382	1.382	1.535	1.222
0.00384	2.113	2.113	1.382	1.382	1.535	1.222
0.00387	2.113	2.113	1.382	1.382	1.535	1.221
0.00389	2.113	2.113	1.382	1.382	1.535	1.221
0.00390	2.113	2.113	1.382	1.382	1.535	1.221

Length of Chip (m)	Electrophoresitic Migration and Flux (mol/m^3)	Electrophoresis Migration (mol/m^3)	Convection, Diffusion, Electrophoretic Migration and Flux (mol/m^3)	Convection and Electrophoretic Migration (mol/m^3)	Diffusion (mol/m^3)	Diffusion and Convection (mol/m^3)
0.00391	2.113	2.113	1.382	1.382	1.535	1.221
0.00394	2.113	2.113	1.382	1.382	1.535	1.221
0.00395	2.113	2.113	1.382	1.382	1.535	1.221
0.00397	2.113	2.113	1.382	1.382	1.535	1.221
0.00400	2.113	2.113	1.382	1.382	1.535	1.221
0.00401	2.113	2.113	1.382	1.382	1.535	1.221
0.00402	2.113	2.113	1.382	1.382	1.535	1.221
0.00404	2.113	2.113	1.382	1.382	1.535	1.221
0.00406	2.113	2.113	1.382	1.382	1.535	1.221
0.00408	2.113	2.113	1.382	1.382	1.535	1.221
0.00409	2.113	2.113	1.382	1.382	1.535	1.221
0.00411	2.113	2.113	1.382	1.382	1.535	1.221
0.00413	2.113	2.113	1.382	1.382	1.535	1.221
0.00414	2.113	2.113	1.382	1.382	1.535	1.221
0.00416	2.113	2.113	1.382	1.382	1.535	1.221
0.00418	2.113	2.113	1.382	1.382	1.535	1.221
0.00420	2.113	2.113	1.382	1.382	1.535	1.221
0.00421	2.113	2.113	1.382	1.382	1.535	1.221
0.00423	2.113	2.113	1.382	1.382	1.535	1.221
0.00425	2.113	2.113	1.382	1.382	1.535	1.221
0.00427	2.113	2.113	1.382	1.382	1.535	1.221
0.00429	2.113	2.113	1.382	1.382	1.535	1.221
0.00431	2.113	2.113	1.382	1.382	1.535	1.221
0.00432	2.113	2.113	1.382	1.382	1.535	1.221

Length of Chip (m)	Electrophoresitic Migration and Flux (mol/m^3)	Electrophoresis Migration (mol/m^3)	Convection, Diffusion, Electrophoretic Migration and Flux (mol/m^3)	Convection and Electrophoretic Migration (mol/m^3)	Diffusion (mol/m^3)	Diffusion and Convection (mol/m^3)
0.00435	2.113	2.113	1.382	1.382	1.535	1.221
0.00436	2.113	2.113	1.382	1.382	1.535	1.221
0.00437	2.113	2.113	1.382	1.382	1.535	1.221
0.00439	2.113	2.113	1.382	1.382	1.535	1.221
0.00440	2.113	2.113	1.382	1.382	1.535	1.221
0.00442	2.113	2.113	1.382	1.382	1.535	1.221
0.00444	2.113	2.113	1.382	1.382	1.535	1.221
0.00446	2.113	2.113	1.382	1.382	1.535	1.221
0.00448	2.113	2.113	1.382	1.382	1.535	1.221
0.00449	2.113	2.113	1.382	1.382	1.535	1.221
0.00451	2.113	2.113	1.382	1.382	1.535	1.221
0.00453	2.113	2.113	1.382	1.382	1.535	1.221
0.00455	2.113	2.113	1.382	1.382	1.535	1.221
0.00457	2.113	2.113	1.382	1.382	1.535	1.221
0.00459	2.113	2.113	1.382	1.382	1.535	1.221
0.00460	2.113	2.113	1.382	1.382	1.535	1.221
0.00463	2.113	2.113	1.382	1.382	1.535	1.221
0.00464	2.113	2.113	1.382	1.382	1.535	1.221
0.00465	2.113	2.113	1.382	1.382	1.535	1.221
0.00467	2.113	2.113	1.382	1.382	1.535	1.221
0.00468	2.113	2.113	1.382	1.382	1.535	1.221
0.00470	2.113	2.113	1.382	1.382	1.535	1.221
0.00472	2.113	2.113	1.382	1.382	1.535	1.221
0.00474	2.113	2.113	1.382	1.382	1.535	1.221

Length of Chip (m)	Electrophoresitic Migration and Flux (mol/m^3)	Electrophoresis Migration (mol/m^3)	Convection, Diffusion, Electrophoretic Migration and Flux (mol/m^3)	Convection and Electrophoretic Migration (mol/m^3)	Diffusion (mol/m^3)	Diffusion and Convection (mol/m^3)
0.00476	2.113	2.113	1.382	1.382	1.535	1.221
0.00478	2.113	2.113	1.382	1.382	1.535	1.221
0.00480	2.113	2.113	1.382	1.382	1.535	1.221
0.00481	2.113	2.113	1.382	1.382	1.535	1.221
0.00483	2.113	2.113	1.382	1.382	1.535	1.221
0.00484	2.113	2.113	1.382	1.382	1.535	1.221
0.00485	2.113	2.113	1.382	1.382	1.535	1.221
0.00488	2.113	2.113	1.382	1.382	1.535	1.221
0.00490	2.113	2.113	1.382	1.382	1.535	1.221
0.00491	2.113	2.113	1.382	1.382	1.535	1.221
0.00492	2.113	2.113	1.382	1.382	1.535	1.221
0.00495	2.113	2.113	1.382	1.382	1.535	1.221
0.00496	2.113	2.113	1.382	1.382	1.535	1.221
0.00498	2.113	2.113	1.382	1.382	1.535	1.221
0.00500	2.113	2.113	1.382	1.382	1.535	1.221
0.00502	2.113	2.113	1.382	1.382	1.535	1.221
0.00504	2.113	2.113	1.382	1.382	1.535	1.221
0.00506	2.113	2.113	1.382	1.382	1.535	1.221
0.00508	2.113	2.113	1.382	1.382	1.535	1.221
0.00509	2.113	2.113	1.382	1.382	1.535	1.221
0.00510	2.113	2.113	1.382	1.382	1.535	1.221
0.00512	2.112	2.113	1.382	1.382	1.535	1.221
0.00514	2.112	2.113	1.382	1.382	1.535	1.221
0.00516	2.112	2.113	1.382	1.382	1.535	1.221

Length of Chip (m)	Electrophoresitic Migration and Flux (mol/m³)	Electrophoresis Migration (mol/m³)	Convection, Diffusion, Electrophoretic Migration and Flux (mol/m³)	Convection and Electrophoretic Migration (mol/m³)	Diffusion (mol/m³)	Diffusion and Convection (mol/m³)
0.00518	2.111	2.113	1.382	1.382	1.535	1.221
0.00519	2.111	2.113	1.382	1.382	1.535	1.221
0.00520	2.111	2.113	1.382	1.382	1.535	1.221
0.00523	2.110	2.113	1.382	1.382	1.535	1.221
0.00524	2.110	2.113	1.382	1.382	1.535	1.221
0.00526	2.109	2.113	1.382	1.382	1.535	1.221
0.00529	2.107	2.113	1.382	1.382	1.535	1.221
0.00530	2.106	2.113	1.382	1.382	1.535	1.221
0.00531	2.105	2.113	1.382	1.382	1.535	1.221
0.00533	2.103	2.113	1.382	1.382	1.535	1.221
0.00535	2.101	2.113	1.382	1.382	1.535	1.221
0.00537	2.098	2.113	1.382	1.382	1.535	1.221
0.00539	2.093	2.113	1.382	1.382	1.535	1.221
0.00540	2.091	2.113	1.382	1.382	1.535	1.221
0.00541	2.088	2.113	1.382	1.382	1.535	1.221
0.00544	2.081	2.113	1.382	1.382	1.535	1.221
0.00546	2.073	2.113	1.382	1.382	1.535	1.221
0.00547	2.065	2.113	1.382	1.382	1.535	1.221
0.00550	2.049	2.113	1.382	1.382	1.535	1.221
0.00551	2.043	2.113	1.382	1.382	1.535	1.221
0.00552	2.033	2.113	1.382	1.382	1.535	1.221
0.00554	2.009	2.113	1.382	1.382	1.535	1.221
0.00556	1.979	2.113	1.382	1.382	1.535	1.221
0.00558	1.960	2.113	1.382	1.382	1.535	1.221

Length of Chip (m)	Electrophoresitic Migration and Flux (mol/m³)	Electrophoresis Migration (mol/m³)	Convection, Diffusion, Electrophoretic Migration and Flux (mol/m³)	Convection and Electrophoretic Migration (mol/m³)	Diffusion (mol/m³)	Diffusion and Convection (mol/m³)
0.00560	1.922	2.113	1.383	1.382	1.535	1.221
0.00561	1.891	2.113	1.383	1.382	1.535	1.221
0.00562	1.869	2.113	1.385	1.382	1.535	1.221
0.00565	1.775	2.113	1.394	1.382	1.535	1.221
0.00565	1.748	2.113	1.398	1.382	1.535	1.221
0.00567	1.691	2.113	1.426	1.382	1.535	1.221
0.00569	1.568	2.113	1.488	1.382	1.535	1.221
0.00572	1.371	2.113	1.912	1.382	1.535	1.221
0.00572	1.348	2.113	1.963	1.382	1.535	1.221
0.00572	1.327	2.113	2.125	1.382	1.535	1.221
0.00575	1.057	2.113	4.152	1.382	1.535	1.221

Table A.2.2 Concentration values at length of the outlet at different potential differences between two inlets for model D

	Concentration (mol/m³) at Zeta Potential (V)								
Out length Length (m)	0	-0.1	0.1	0.3	-1.1	-0.9	-0.7	-0.5	-0.3
0	3.486	4.135	2.854	1.636	6.886	6.908	6.915	6.852	5.483
5.6E-06	3.479	4.127	2.848	1.632	6.881	6.901	6.907	6.842	5.474
1.2E-05	3.421	4.061	2.798	1.601	6.812	6.824	6.821	6.749	5.393
3.7E-05	3.394	4.033	2.774	1.586	6.840	6.837	6.819	6.731	5.367
7.0E-05	3.314	3.938	2.708	1.547	6.729	6.714	6.681	6.584	5.244
1.1E-04	3.595	4.271	2.939	1.681	7.244	7.239	7.218	7.123	5.681
1.4E-04	3.495	4.152	2.858	1.635	7.057	7.045	7.020	6.926	5.522
1.8E-04	3.460	4.112	2.827	1.615	6.972	6.971	6.953	6.865	5.474
2.1E-04	3.427	4.070	2.801	1.602	6.899	6.898	6.880	6.792	5.416
2.4E-04	3.364	3.993	2.751	1.574	6.722	6.729	6.720	6.643	5.305
2.4E-04	3.406	4.041	2.788	1.597	6.764	6.778	6.777	6.707	5.362
2.5E-04	3.408	4.043	2.790	1.599	6.761	6.777	6.777	6.708	5.364
Average	3.437	4.081	2.811	1.609	6.881	6.885	6.874	6.794	5.424

Table A.2.3 Concentration at Outlet length at different zeta potential values for model D

Outlet Length (m)	Concentration (mol/m³) at Zeta Potential (V)			
	0.1	0.2	0.3	0.4
0	2.350	3.796	5.483	7.281
5.6E-06	2.356	3.801	5.474	7.246
1.2E-05	2.370	3.799	5.393	7.017
3.7E-05	2.455	3.903	5.367	6.815
7.0E-05	2.543	3.944	5.244	6.562
1.1E-04	2.639	4.186	5.681	7.124
1.4E-04	2.628	4.118	5.522	6.917
1.8E-04	2.564	4.037	5.474	6.869
2.1E-04	2.460	3.923	5.416	6.932
2.4E-04	2.365	3.766	5.305	6.880
2.4E-04	2.348	3.757	5.362	7.053
2.5E-04	2.342	3.750	5.364	7.076